PERFORMANCE STUDY OF TWO-STAGE-TO-ORBIT REUSABLE LAUNCH VEHICLE PROPULSION ALTERNATIVES

THESIS

Marc A. Brock, Captain, USAF

AFIT/GSS/ENY/04-M02

DEPARTMENT OF THE AIR FORCE
AIR UNIVERSITY

AIR FORCE INSTITUTE OF TECHNOLOGY

Wright-Patterson Air Force Base, Ohio

The views expressed in this thesis are those of the author and do not reflect the official policy or position of the United States Air Force, Department of Defense, or the United States Government.

AFIT/GSS/ENY/04-M02

PERFORMANCE STUDY OF TWO-STAGE-TO-ORBIT REUSABLE LAUNCH VEHICLE PROPULSION ALTERNATIVES

THESIS

Presented to the Faculty

Department of Aeronautics and Astronautics

Graduate School of Engineering and Management

Air Force Institute of Technology

Air University

Air Education and Training Command

In Partial Fulfillment of the Requirements for the

Degree of Master of Science (Space Operations)

Marc A. Brock, BS, ME

Captain, USAF

March 2004

AFIT/GSS/ENY/04-M02

PERFORMANCE STUDY OF TWO-STAGE-TO-ORBIT REUSABLE LAUNCH VEHICLE PROPULSION ALTERNATIVES

Marc A. Brock, BS, ME
Captain, USAF

Approved:

Milton E. Franke (Chairman)	date
Ralph A. Anthenien (Member)	date
Paul I. King (Member)	date

Abstract

This study investigated the performance of five Two-Stage-To-Orbit reusable launch vehicles (RLV), with stages propelled by rocket engines, turbojet engines and Rocket Based Combined Cycle (RBCC) engines. Horizontal versus vertical takeoff launch and direct versus lifting ascent trajectories were also studied. A method was conceived using a 3 degree of freedom optimization program, stage inert mass fractions, and a fixed gross takeoff weight (GTOW) of 1,000,000 lbf to determine each RLVs performance based on payload weight delivered to orbit and total vehicle inert weight. RLV trajectory constraints, mass fractions, engine performance, and aerodynamics were assumed from literature of similar RLVs or data provided by the Air Force Research Laboratory (AFRL). The method devised predicted performance for all RLVs studied, but was time intensive and intolerant of small trajectory modifications. A horizontal takeoff RLV with the 1st stage powered by turbojet engines and the 2nd stage propelled by a rocket engine, in a lifting ascent trajectory, provided 3 times the payload weight to orbit when compared to the same vehicle in a vertical takeoff mode. The RLV with both stages propelled by rocket engines lifted more payload weight into orbit with a lower inert weight than all other RLVs studied. RLVs propelled by RBCC engines, on a direct ascent trajectory, had insufficient fuel to reach orbit because of the high inert weight of the RBCC engines.

Acknowledgments

I would like to express my sincere appreciation to my faculty advisor, Dr. Milton Franke, for his guidance and support throughout the course of this thesis effort. The insight and experience was certainly appreciated. I would, also, like to thank my sponsors, Capt. Christopher Hamilton and Dr. Dean Eklund, from the Air Force Materiel Command for both the moral and intellectual support provided to me in this endeavor.

I am also indebted to my many fellow students whom had the good the manners to laugh at my numerous poorly timed and ill-conceived attempts at humor. They ensured that the educational experience was entertaining.

Finally, I must thank my wife and children for their unwavering support during my grueling thesis experience. My wife, kept cracking the whip and ensured that I remained focused. My children kept me laughing and helped me to remember that there is much more to life than thesis research. Coincidentally, through my children I learned that reading the Dr. Seuss book, Fox In Socks, is infinitely more difficult than any rocket science.

Marc A. Brock

Table of Contents

Page

Page

List of Figures

List of Tables

Table Page

Page

Nomenclature

Symbol	Description
A_e	Nozzle Exit Area (ft^2)
AFRL	Air Force Research Laboratory
APTSS	Aerospace Propulsion Technology Screening Study
$[\cos(?)]_{ave}$	Average of the Cosine of the Flight Path Angle
C_D	Drag Coefficient
C_L	Lift Coefficient
D	Drag Force (lbf)
? V	Change of Velocity (ft/sec)
?	Density (lbm/ft^3)
DoD	Department of Defense
ESJ	Ejector Scramjet
F_1	1^{st} Stage Inert Mass Fraction
F_2	2^{nd} Stage Inert Mass Fraction
GTOW	Gross Takeoff Weight (lbf)
HRE	Hypersonic Research Engine
ICBM	Intercontinental Ballistic Missile
Isp	Specific Impulse (sec)
Isp_a	Average Specific Impulse Over Entire Stage Burn Time (sec)
L	Lift Force (lbf)
lbf	pounds force

lbm	pounds mass
$\dot{m}$	Exhaust Mass Flow Rate (lbm/sec)
$\dot{m}_a$	Air Mass Flow Rate (lbm/sec)
$\dot{m}_f$	Fuel Mass Flow Rate (lbm/sec)
NAI	National Aerospace Initiative
NASA	National Aeronautics and Space Administration
NASP	National Aerospace Plane
p_a	Ambient Pressure (lbf/ft^2)
p_e	Exhaust Pressure (lbf/ft^2)
POST	Program to Optimize Simulated Trajectories
RBCC	Rocket Based Combined Cycle
RLV	Reusable Launch Vehicle
S	Lifting Surface Reference Area (ft^2)
SAM	Structural Assembly Model
SERJ	Supercharged Ejector Ramjet Engine
SESJ	Supercharged Ejector Scramjet Engine
SLI	Space Launch Initiative
SSME	Space Shuttle Main Engine
SSTO	Single Stage to Orbit
?	Flight Path Angle Measured From Vertical (deg)
t_b	Stage Burn Time (sec)

T	Thrust Force (lbf)
T/W	Thrust to Weight
TAV	Trans-atmospheric Vehicle
TBCC	Turbine Based Combined Cycle
TPS	Thermal Protection System
TSTO	Two Stage to Orbit
USAF	United States Air Force
u	Velocity (ft/sec)
u_e	Exhaust Velocity (ft/sec)
u_{eq}	Equivalent Velocity (ft/sec)
W	Weight (lbf)
W_b	W_o – Stage Fuel Weight (lbf)
W_{inert1}	1st stage inert weight (lbf)
W_{inert2}	2nd stage inert weight (lbf)
$W_{initial2}$	2nd stage initial weight (lbf)
W_o	Total Stage Weight (lbf)
W_{orbit}	Propellant weight at orbit insertion from POST output (lbf)
W_{pay}	Payload Weight (lbf)
W_{prop1}	1st stage propellant weight (lbf)
W_{prop2}	2nd stage propellant weight (lbf)
W_{stg}	Staging condition vehicle weight (lbf)
W_{tot1}	1st stage total weight (lbf)

W_{tot2}	2^{nd} stage total weight (lbf)

PERFORMANCE STUDY OF TWO-STAGE-
TO-ORBIT REUSABLE LAUNCH VEHICLE PROPULSION ALTERNATIVES

1. Introduction

1.1 Motivation

Since the inception of spaceflight the United States Air Force (USAF) and the National Aeronautics and Space Administration (NASA) have searched for an affordable, routine, and operationally responsive launch system to provide access to space. For the past five decades, both agencies have relied on expensive, non-responsive expendable launch vehicles and the Space Shuttle to meet their space access needs. Over that duration, NASA and the Air Force studied numerous reusable launch vehicle (RLV) architectures and technologies, yet none reached operational capability. These doomed RLV programs were hampered by technological hurdles, political adversaries and spiraling program costs (5).

Recently, both agencies decided once more to develop a RLV that will meet their evolving launch requirements (10:71). These new RLV programs attempt to capitalize on technological innovations in propulsion and advanced thermal protection systems (5). Political barriers may also be dissipating in the wake of Space Shuttle Columbia disaster as politicians call for a new RLV to replace the aging shuttle fleet. The President and military leaders also recognize the

need for a quick response military space vehicle for spacelift and space force application (28: 67-68). Although there are no firm indications that innovative technology will reduce RLV costs, the political impetus created by the need to replace the Space Shuttle may outweigh the enormous cost of a new RLV.

With this renewed civil and military interest in a RLV, researchers intensified the debate over the optimal propulsion configuration for a RLV. While most researchers agree that any near-term RLV must be a Two-Stage-To-Orbit (TSTO) vehicle, industry and academics are promoting various engine systems to propel a new RLV. Proposed propulsion systems include: airbreathing engines; combined propulsion systems like Rocket Based Combined Cycle (RBCC) engines and Turbine Based Combined Cycle (TBCC) engines; and rocket based engines. Airbreathing engines include ramjets, scramjets, and turbine engines. Rocket based engines include pure rockets and air-augmented rockets that entrain incoming air-flow to increase engine performance. RBCC engines combine a Rocket Based engine and a ramjet or scramjet engine in a single flow-path. TBCC engines combine a turbine engine and a ramjet or scramjet engine in a single engine casing.

Additionally there is disagreement over the launch and landing technique, whether horizontal or vertical; the staging Mach number; and other trajectory constraints for an RLV launch. The performance of any RLV propulsion system will depend on all of these variables. This study is an attempt to provide an unbiased analysis of these various propulsion configurations.

1.2 Research Objectives

There were three objectives to this study. The first purpose of the research was to create an accurate methodology to analyze RLV performance across a wide spectrum of propulsion and vehicle configurations. The second purpose was to determine if the proposed methodology, using the 3 degree of freedom trajectory optimization program, could be used to analyze the effects of various trajectory constraints on vehicle performance. The trajectory constraints studied include: staging dynamic pressure, maximum dynamic pressure, maximum g-limit, and staging Mach number. The third purpose was to compare five different conceptual TSTO RLV configurations from the Air Force Research Laboratory (AFRL) Aerospace Propulsion Technology Screening Study (APTSS) to determine which of the five RLV's yielded the best performance. The primary performance figures of merit were the total inert weight of the launch vehicle and the payload weight that the vehicle could lift into low earth orbit, given a fixed gross takeoff weight. The study included computational analyses of airbreathing, rocket, and combined propulsion systems ready for military operations within the next 10 years. A 3 degree of freedom trajectory-optimization computer program was used to conduct the analysis. Both vertical and horizontal takeoff launch techniques were considered.

1.3 Thesis Overview

This work is organized into five chapters along with three appendices. Chapter 2 contains a cursory literature review on the history and background of various RLV propulsion systems and configurations. Chapter 3 provides the methodology and computer program used to analyze the propulsion systems. Chapter 4 presents the results of the study. Chapter 5

provides conclusions on the results and recommends future study. All data presented in this paper were in English units. English units were found to be the industry standard for RLV research.

2. Literature Review

A preliminary research step was study of past and present RLV programs. Although most of these past systems did not reach operational status, they provide insight into the evolution of RLVs and detail what propulsion technologies may be effective for RLV use. Current RLV programs and research indicate where RLV programs may be in the next 10 years. They also reveal government trends and desires for future RLV programs. Modern RLV technology studied include: airbreathing systems, rocket based systems and combined propulsion systems.

2.1 Reusable Launch Vehicle Background

The Air Force and NASA spent considerable effort on RLV technology demonstrations since the first attempted RLV, the 1960s Dyna Soar vehicle. The Dyna Soar manned RLV, derived from the Titan Inter-Continental Ballistic Missile (ICBM), was to serve as a satellite interceptor vehicle but failed to become operational. The Dyna Soar was cancelled in 1962, about three years before scheduled flight, due to a poorly designed military mission and DoD desire to design a different space vehicle (9: 5-6).

Following Dyna Soar, the USAF decided that military space vehicles must operate like an airplane, with horizontal takeoff and landing. The Air Force conducted the Transatmospheric Vehicle (TAV) studies in the 1980s to investigate technologies for such an aerospace plane. The program investigated rocket and air-breathing Single-Stage-To-Orbit (SSTO) and TSTO vehicles. Two out of three TAV SSTO test vehicles failed during testing due to excessive weight, while one vehicle was launched with limited success. The successful vehicle failed

during testing due to a manufacturing defect. Although the defect was easily correctable, the program was terminated in 1988 (5: 2-5, 13).

Following the TAV studies, the Department of Defense (DoD) and NASA jointly researched RLV technology through the National Aerospace Plane (NASP) program. The NASP program lasted from 1986 to 1994 without producing a flight-worthy space plane, and was terminated during post cold-war budget cuts. Additionally, the NASP vehicle velocity was 3,000 feet per second short of reaching orbital speed (9: 8). While the vehicle failed, some program achievements included: design and ground test of combined cycle engine components; design and subscale test of a linear rocket; development of high temperature materials; and production of slush hydrogen (5: 5-6).

NASA attempted two rocket-powered RLV technology demonstration vehicles in the 1990s: the X-33 and X-34. The X-33, a subscale SSTO technology demonstrator, was a joint venture between NASA and industry. The X-33 program goal was to reduce SSTO development risk significantly to enable private investment in a full-scale operational vehicle. The program was terminated due to funding and technology problems prior to achieving flight. The X-34, a Mach 8 vehicle designed to test advanced technologies, fell behind schedule and suffered from spiraling costs. Like the X-33 program, it was also terminated prior to flight. These programs bolstered NASA's belief in airbreathing propulsion for RLV applications, while shifting focus from SSTO to TSTO vehicles (5: 5-6).

NASA and the Air Force continued the quest for viable RLV technology through joint efforts. Both agencies collaborated on the X-43 hypersonic demonstration vehicle which,

among other goals, was designed to test hydrogen-fueled scramjet technologies at speeds up to Mach 10. Although the first X-43 flight failed in June 2002, successive tests are planned over the next decade (24). In 2002 NASA and the Air Force conducted a 120-day joint study of RLV concepts to address joint requirements aimed at reducing development costs. The study concluded that TSTO technology is feasible in the short-term, and both agencies continue to work toward that goal today (5: 6). NASA and the DoD formalized their RLV development cooperation under the National Aerospace Initiative (NAI) program. The NAI program is charged to develop and demonstrate: safe, reliable and affordable technologies; airbreathing hypersonic technology; and responsive in-space capabilities (25).

NASA's current attempt to develop a RLV is rooted in the Space Launch Initiative (SLI) program under the auspices of the Next Generation Launch Technology program. This program consists of three generations of RLV advancements. The 1st Generation RLV program involves upgrading the existing Space Shuttle program to increase reliability and lower cost. The 2nd Generation RLV program strives to develop a mid-term Space Shuttle replacement using a TSTO vehicle by 2012. NASA plans to develop a SSTO RLV under the 3rd Generation RLV program by 2025. The space agency hopes this effort will reduce launch costs to $100 per pound of payload and increase reliability by a factor of 10^4 over current launch vehicles (5: 5-6; 23). The Space Shuttle Columbia accident in 2003 places greater pressure on NASA to fulfill these goals.

While the Air Force is working with NASA to develop common RLV technologies, the Air Force's RLV requirements are quite different than NASA's. The USAF and the

Department of Defense (DoD) require an operationally responsive spacelift capability to ensure American space superiority. This mandate, set forth by Air Force doctrine requires the military develop and procure a space launch system that meets the nation's evolving spacelift and space control needs. The doctrine specifically recommends that the Air Force examine RLV technology to meet America's space requirements (8). The Air Force is specifically researching TSTO spaceplane configurations to meet this need by 2014 (5).

2.2 Rocket Based Propulsion

Rocket based propulsion, conceived almost 100 years ago, has powered all operational American spacelift vehicles since the inception of the space program. Rocket Based propulsion includes pure rockets and air-augmented rockets. Both types of rocket engines carry all the fuel and oxidizer needed to provide thrust, while air-augmented rockets increase propulsive efficiency by entraining ambient air into the engine. Both liquid and solid rocket engines are used in modern spaceflight applications and may be used in any future RLV program. Air-augmented rockets show potential for RLV applications as well.

Rocket Based propulsion systems offer both benefits and drawbacks for RLV applications. Their prime operational benefit is that they provide thrust during an entire flight regime: from static takeoff, through the earth's atmosphere, and into the vacuum of space. There is no Mach number limitation on their operation which allows them to accelerate a launch vehicle to orbital speed. They also have a high thrust-to-weight (T/W) ratio which provides for vertical takeoff. The major drawback to rocket engines is that the RLV must carry all the oxidizer on-board, thus increasing gross weight of the launch vehicle (7: 5).

2.2.1 Liquid Rocket Propulsion

Monopropellant and bipropellant systems are the primary liquid rocket propulsion methods. In a monopropellant rocket a hypergolic propellant, like hydrazine, flows over a catalyst bed to exothermically decompose and provide thrust. Monopropellant specific impulse (Isp) values range from 150 to 230 seconds, depending on the propellant, and are most often used for in-space propulsion. A bipropellant rocket engine contains separate tanks for liquid fuel and oxidizer. The fuel and oxidizer are pumped into an engine where mixing and combustion occurs. The hot gases are accelerated out an exhaust nozzle to provide thrust. Typical liquid rockets use liquid oxygen (LOx) as the oxidizer and RP-1, a kerosene based fuel, or liquid hydrogen (LH_2) as the fuel (19: 188-189). These systems provide greater Isp values than monopropellant rockets, in the range of 290 to 450 seconds, depending on the propellant and oxidizer mixture (19: 695-714). A RP-1 and LOx bipropellant engine powered the first stage of the Saturn V vehicle. The reusable Space Shuttle Main Engines (SSME) uses LOx and LH_2 (17: 189).

Liquid rockets are ideal for RLV applications because they are well-known, space-tested, and reliable engines. They can operate intermittently, allowing throttling, shutdown, and start-up to maximize performance over flight duration (19: 188-189). Researchers believe these engines can be useful in future RLVs to propel upper stage vehicles out of the atmosphere or to

accelerate first-stage vehicles utilizing airbreathing engines, like scramjets, that require high speeds to operate (13: 6).

2.2.2 Solid Rocket Propulsion

Unlike liquid rocket engines, the fuel and oxidizer in a solid rocket propulsion system are combined as a solid substance prior to launch. The solid mixture is stored in the combustion chamber of the rocket and ignited when needed. The hot combustion products accelerate out the exhaust nozzle to produce thrust. Common propellants include: zirconium, titanium, boron, and aluminum. Ammonium perchlorate and ammonium nitrate are the two most frequently used oxidizers (19: 325). Isp values for solid rockets are usually less than liquid engines. Solid rocket engines are often used for ICBMs because they require little maintenance once filled. They are used in most domestic launch vehicles as a first stage or strap-on booster (19: 297).

Like liquid rocket engines, solid rockets are a trusted space launch asset that may be useful to future RLV programs. Their high density propellant/oxidizer mixture requires a smaller volume when compared to liquid rocket engines (19: 297). This may be useful to reduce RLV structural mass. Solid rocket burning rates can be varied to provide optimal thrust throughout a planned trajectory by grain geometry of the mixture (19: 333). Unfortunately, once a solid rocket begins burning it is difficult to stop the combustion process. Solid rockets are also difficult to manufacture, handle and throttle and they often produce toxic exhaust (19: 4).

2.2.3 Air-Augmented Rocket Propulsion

Air-augmented rockets, also called ramrockets, utilize incoming airflow to enhance traditional rocket combustion. The additional airflow increases the mass flow rate and ultimately

improves performance over traditional rockets. Unlike airbreathing engines, these engines produce thrust throughout an entire flight regime, from takeoff to the vacuum of space. A simple ramrocket, as depicted in Figure 1, has both a rocket and secondary combustion chamber. A fuel-rich mixture of fuel and oxidizer burns in the rocket combustion chamber. The fuel-rich exhaust gases then combust a second time with the incoming entrained airflow in the secondary combustion chamber. The resulting flow is accelerated out the exhaust nozzle. The ramrocket depicted in Figure 1 is one of many different configurations of air-augmented rockets (19: 632-634). Additionally, AFRL is investigating the feasibility of supersonic ramrockets, or scramrockets, to propel vehicles at hypersonic speeds (31).

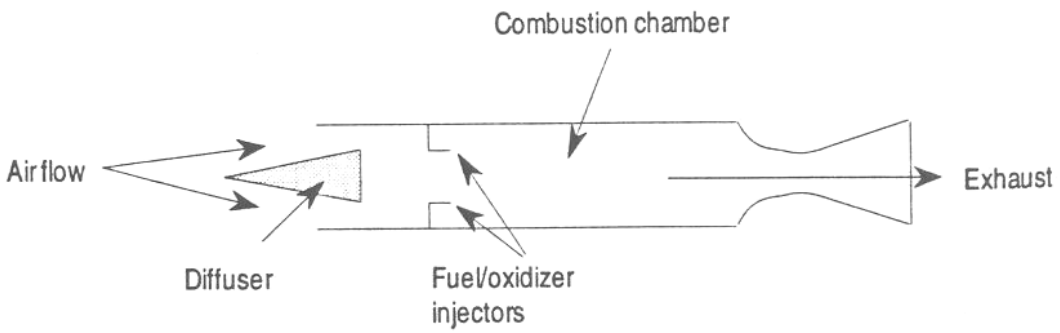

Figure 1: Basic Ramrocket (19: 632)

2.3 Airbreathing Propulsion

The realm of airbreathing propulsion for RLV applications consists of turbine engine, ramjet and scramjet technology. RLV researchers believe that these systems can augment rocket engines and propel a RLV through a portion of the atmosphere. According to V.J. Bilardo of the NASA Langley Research Center, airbreathing propulsion has three

characteristics that make it suitable to provide cost-effective, reliable access to space. These three characteristics include: low sensitivity to weight growth when compared to rocket systems; superior launch, flight, and ground operability over rockets; and vast room for airbreathing engine advancement when compared to the mature state of rocket technology (3: 2-3).

Bilardo also acknowledges that there are numerous drawbacks to airbreathing engines. Airbreathing engines are projected to be 4 to 5 times heavier than rocket engines for the same thrust. They require larger fuel tanks due to the lower fuel bulk density. An RLV powered by airbreathing engines will require a heavier thermal protection system (TPS) compared to a rocket-powered RLV due to the high dynamic pressure ascent trajectory. The airbreathing RLV weight will also increase from the addition of wings, body and gear designed for a fully-loaded takeoff (3: 3).

2.3.1 Turbine Based Engines

Turbine based engines, a well-known and reliable propulsion application, have been used in aircraft operations for the last 60 years. Turbine based engines, capable of supersonic flight, powered aircraft like the Air Force's F-15 Eagle and the Concord passenger plane. A typical turbojet engine, as shown in Figure 2, consists of several rotary compressor blades to increase the pressure of the incoming freestream air. The compressed air travels through a diffuser en route to the combustor. Following combustion, the air flows through the rotary turbine blades to power the compressor. The flow then exits through an expansion nozzle to produce thrust (18: 145).

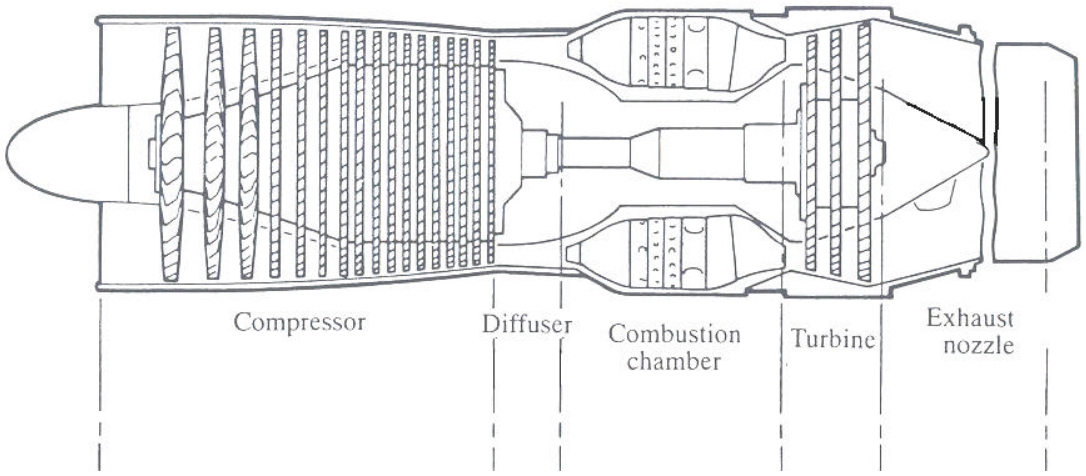

Figure 2: Typical Turbojet Engine Configuration (18: 145)

Turbojet engines yield numerous advantages for RLV design. Turbojet Isp can range from 2000 to 4000 seconds. This is an order of magnitude greater than rocket based engines and the highest of all propulsion technologies discussed. This Isp advantage will result in significantly lower propellant consumption (29: 2). Turbojets provide low-speed power for initial acceleration and powered descent in addition to supersonic cruise. This capability provides a wide range of benefits to include: power loiter, approach and landing with go-around capability, self ferry for the vehicle to return to home base after landing, and controlled abort following launch. Ultimately, turbine engines use may reduce the gross takeoff weight (GTOW) of a RLV when compared to a rocket-powered vehicle (13: 2, 4, 17).

There are several drawbacks to the turbojet in RLV applications. The turbojet's main disadvantage for RLV use is its reduced capacity to propel a vehicle to hypersonic speeds.

Turbojet complex rotating machinery is susceptible to wear and requires more maintenance than ramjets and scramjets. This machinery also adds dry weight to the turbojet when compared to other systems. The low T/W ratio of turbojets also increases system dry weight when compared to Rocket Based engines. These engines are normally larger than rocket engines for the same amount of thrust (29: 3).

NASA is investigating the use of turbine engines for a RLV application through the Revolutionary Turbine Accelerator (RTA) program. The RTA program goal is to design a high-speed turbine engine that can propel a RLV to speeds greater than Mach 4. These advanced turbine engines are projected to have Isp values ranging from 300 to 3000 seconds depending on flight speed. NASA believes that this technology can be used to power the first stage of a TSTO RLV. The RTA engine is scheduled for ground testing in 2006 (12: 2).

2.3.2 Ramjets

Ramjets are a reliable engine that the military has utilized for over 50 years in missiles and airplanes. These engines excel in supersonic flight in the Mach number range of 3-6. The basic ramjet engine, detailed in Figure 3, consists of a simple design with no rotating machinery. Freestream air enters the engine inlet, where a series of oblique and normal shock waves reduce the flow velocity to subsonic speeds, while compressing the incoming air. The subsonic air is then combusted and accelerated out the exhaust nozzle to produce thrust (17: 22-23).

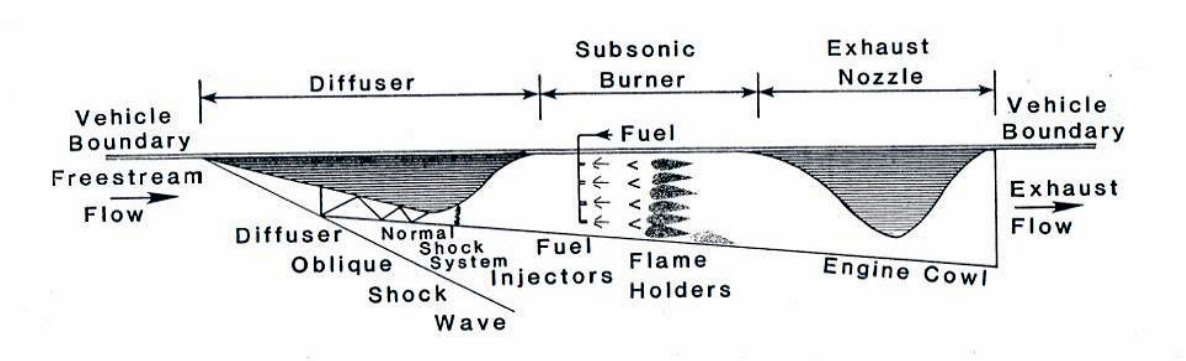

Figure 3: Typical Ramjet Engine Configuration (17: 23).

There are various advantages and disadvantages to ramjet use in RLV operations. The ramjet engine is less complex than a turbojet engine because there are no rotating turbines or compressors. Ramjets are also inherently lighter than rocket engines because they do not carry oxidizer. Ramjet specific impulse ranges from 1000 to 2000 seconds. This is much greater than typical rocket performance but considerably less than turbine engine Isp values (29: 2). Unfortunately, ramjets cannot produce thrust from a stopped position or in a vacuum. They must be accelerated to near Mach 4 by some other means, like a turbojet or rocket, to reach an acceptable velocity to efficiently produce thrust (17: 3, 22-23; 18: 164).

2.3.3 Scramjets.

Scramjets have been studied in depth since the 1960s. Engineers ground tested scramjet engines under various past RLV programs, and they recently began flight tests on these engines. Scramjets are designed to operate at Mach numbers greater than six. In a scramjet engine configuration, as shown in Figure 4 the incoming air-flow is partially compressed and

decelerated via series of oblique shock waves. The incoming air-flow is then mixed with fuel and combusted at supersonic speeds. Following supersonic combustion the flow accelerates out the exhaust nozzle creating thrust. Supersonic combustion reduces excessive losses due to normal shocks, wall heat transfer, and chemical dissociation. These losses are associated with ramjet operation at Mach numbers above six (17: 23-24).

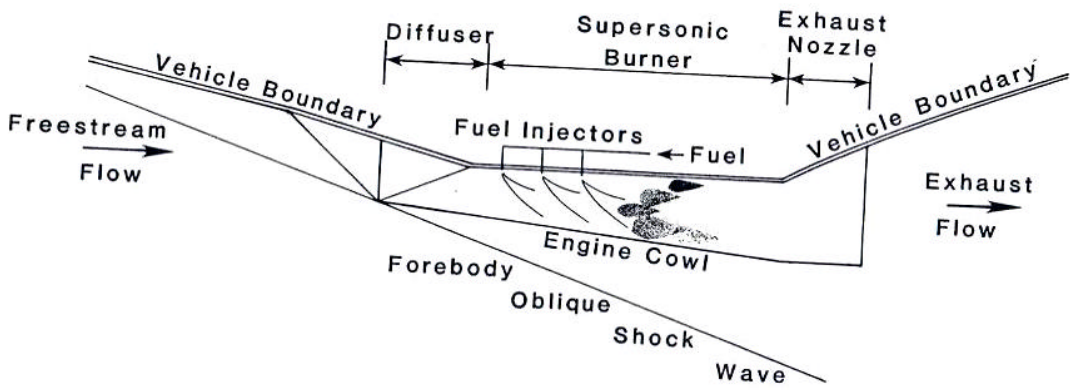

Figure 4: Typical Scramjet Engine Configuration (17: 24)

Scramjets share all of the advantages of ramjets for use in RLV applications, with some additional benefits. The primary scramjet benefit is that they operate at hypersonic speeds up to Mach 15. Therefore, a scramjet-powered RLV may only require an additional 10,000 feet per second in velocity from a secondary engine to reach a low earth orbit velocity of approximately 25,500 feet per second (13: 3). Scramjet Isp values range from 1000 to 1500 seconds, 5

times greater than rocket Isp values. Supersonic combustion within the scramjet provides lower internal pressure and heat transfer rates thus easing the structural requirements on the combustor (17: 23-24). These engines can also be designed in a dual-mode that allows both scramjet and ramjet operation in one engine. This feature provides a greater operating range for the engine (12: 152).

Unfortunately, the supersonic combustion complicates the combustion process and the overall vehicle design. The combustor must be designed to mix fuel and air rapidly to ensure combustion prior to the flow exiting the engine. Additionally, small scramjet engines cannot be attached to the RLV's wings or aft, because early scramjet research determined that axisymmetric wing-mounted engines produced prohibitively large drag on pylons and inlet cowls. In these engines internal flow was dominated by wall effects which reduced engine performance. To mitigate these problems, the scramjet engine must be integrated into the body of the RLV. This will ensure large scramjet inlet area, utilize the RLV body for leading edge compression and trailing edge expansion, and reduce internal and external drag. For the reasons listed above, most proposed scramjet-powered vehicle designs are similar to that shown in Figure 5. As Figure 5 shows, the scramjet is attached to the underside of the craft. The fore-body of the aircraft produces oblique shock waves and guides a large amount of air into the inlet. The entire aft section of the aircraft is sloped to act as an expansion surface to accelerate the exhaust flow. (17: 23-25).

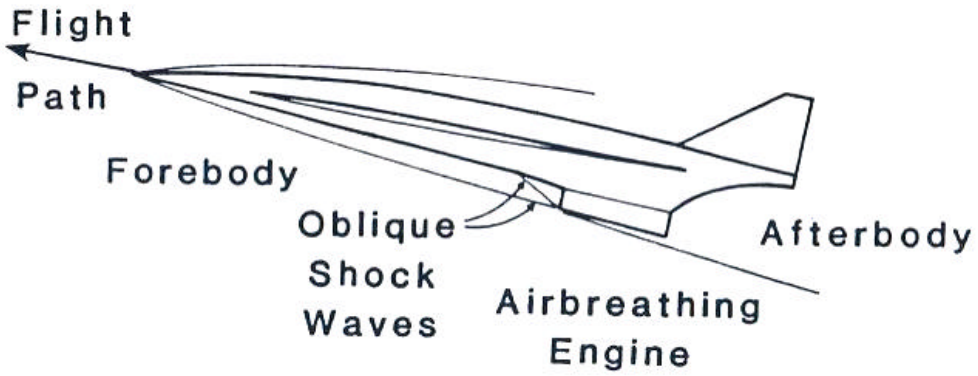

Figure 5: Typical Scramjet-Powered Vehicle Configuration (17: 25)

In 1964 NASA and the Air Force began the first scramjet testing for airplane operations through the Hypersonic Research Engine (HRE) Project. The goal of the project was to flight test the HRE engine on the X-15-A aircraft. An HRE program ramjet engine flew several times, un-powered, attached to underside of the X-15-A. Unfortunately, the HRE flight-test program was cancelled, prior to powered flight testing of the scramjet engine, with the termination of the X-15-A program in 1968. The HRE program persisted through ground-testing in wind tunnel facilities at NASA Langley until the project was terminated in 1975 (2: 2).

Although the HRE program never reached flight status, a complete flight weight and regeneratively cooled Structural Assembly Model (SAM) scramjet was constructed and tested at simulated conditions of Mach 7 flight in NASA Langley's High Temperature Structures Tunnel. A second HRE engine was also built and tested at simulated flight conditions ranging from Mach 5 through 7 in the NASA Lewis Hypersonic Tunnel Facility. These tests revealed technical difficulties with scramjet engines to include: achieving and maintaining efficient mixing

and combustion; the importance of accounting for external drag; the complications of performing under a wide operating range; and the need for realistic ground testing facilities (17: 12-13).

NASA and the Air Force are researching scramjet engines for RLV propulsion through the X-43 Hyper-X project. The main goal of this program is to flight-demonstrate the airframe-integrated ramjet/scramjet engine. A converted B-52 will lift the unmanned X-43 vehicle, shown in Figure 6, to 40,000 feet in altitude. A modified Pegasus rocket will boost the X-43 to 100,000 feet and supersonic speeds. Following rocket separation, the X-43 will fly under its own power for up to 6 minutes to collect hypersonic data prior to controlled descent. NASA will use the data to validate scramjet propulsion and hypersonic aerodynamics over the range of Mach 5 through Mach 10 (24: 2-3).

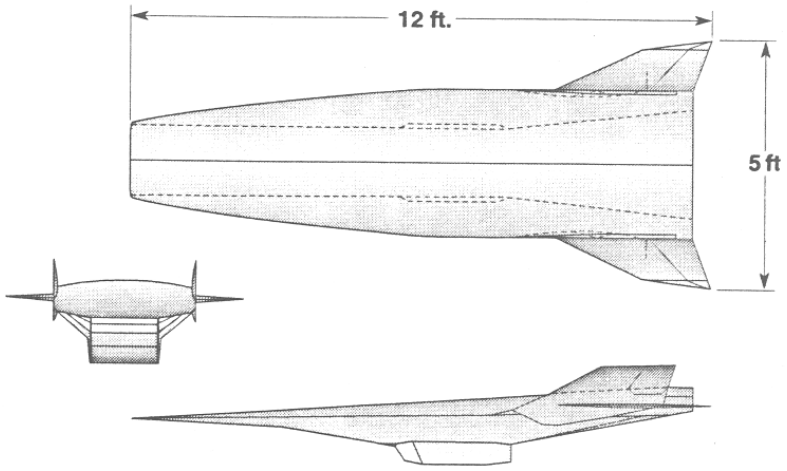

Figure 6: Hyper-X Vehicle Configuration (24: 2)

2.4 Combined Cycle Airbreathing and Rocket Propulsion

The most promising propulsion configurations for RLV applications are combined cycle systems. These engines, in the embryonic development stages, unite both rocket and airbreathing propulsion modes into a single system. Most combined cycle engines unite airbreathing and rocket systems synergistically into a single engine case to improve overall system performance. Combined cycle engines operate over an expanded Mach and altitude range when compared to pure airbreather operation alone. The versatile nature of these engines allows for controlled powered flyback and abort capability for a RLV (13: 1).

Many of the combined cycle engines studied today were derived in the 1960's by the Mardquart Company under contract from NASA. Mardquart's nine-volume report examined the feasibility and performance potential of over 30 different combined propulsion systems. Rocket engineers have studied these engines intensely since the 1960's, yet none of the Mardquart engines have reached operational status. All the engines detailed by Mardquart, and more conceived in the last four decades, are either Turbine Based or Rocket Based Combined Cycle engines (14: 2-3).

2.4.1 Rocket Based Combined Cycle Engines

RBCC engines typically join a Rocket Based propulsion system with a ram/scram airbreathing engine in a single flow path. These engines are similar in architecture and performance to air-augmented rockets like ramrockets and scramrockets. RBCC engines operate over the entire Mach and altitude range needed for RLV trajectory to orbit. RBCC engines are typified by the ejector scramjet (ESJ) engine, studied by Mardquart in the 1960s, shown in Figure 7 (13: 8). The ESJ engine is capable of operating over the entire flight regime

for a RLV, from takeoff to orbit insertion. The ESJ has four distinct operating modes, as shown in Figure 8: air-augmented rocket, ramjet, scramjet, and pure rocket. The air-augmented rocket is used to accelerate the vehicle from takeoff up to Mach 2.5 or Mach 3. This mode's high thrust allows for vertical or horizontal takeoff scenarios. The engine then ceases rocket combustion and converts to the significantly higher Isp ramjet mode. Near Mach 6 the engine converts operation to scramjet mode in order to reduce losses from internal heating and friction. In the range of Mach 10 through Mach 15 the inlet closes, the vehicle pitches up, and the engine operates in pure rocket mode until main engine cutoff for orbit insertion (13: 8-11).

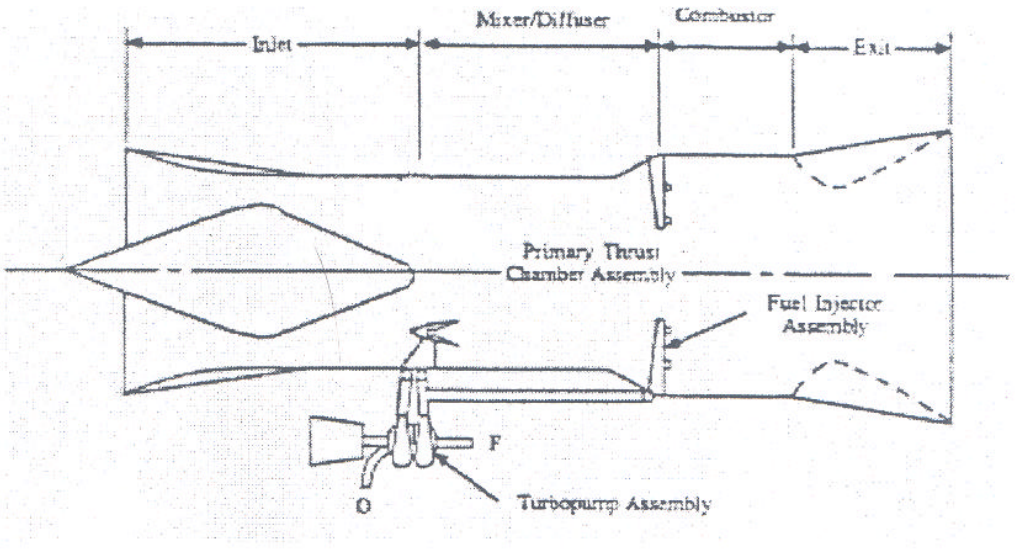

Figure 7: Mardquart Ejector Scramjet Engine Design (26: 8)

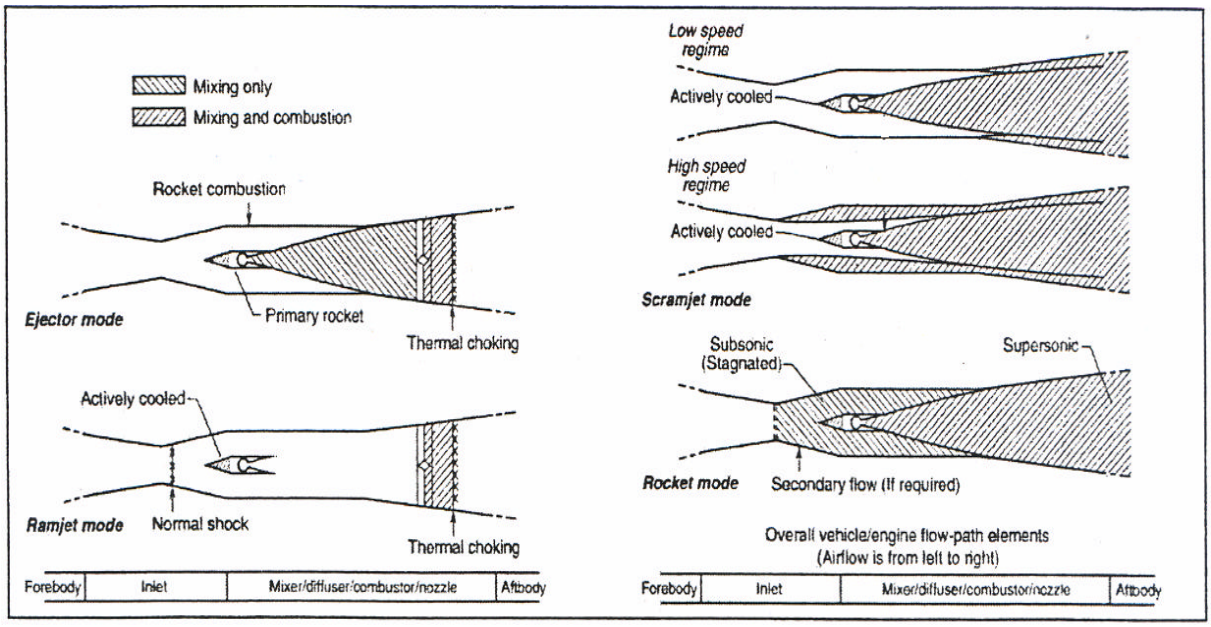

Figure 8: Mardquart Ejector Scramjet Engine Modes (26: 9)

Although the RBCC technology readiness is low, many aerospace companies and NASA are pursuing the high performance potential of these engines. Currently, companies like Boeing and Aerojet are working to build an operational RBCC to meet the need. NASA, through the Integrated System Test of an Air-breathing Rocket (ISTAR) program, is scheduled to begin flight-testing of its own RBCC in 2008 (22: 3).

2.4.2 Turbine Based Combined Cycle Engines

Turbine Based Combined Cycle engines combine a low-speed turbine engine with a higher speed ramjet or scramjet and perhaps an air-augmented rocket as well. These propulsion systems are the furthest from development and most technically complex, when compared to those detailed above, yet they hold the most potential performance benefits for RLV applications. TBCC engines are either single flow-path or dual flow-path engines. They

are ideal for first stage operations on a TSTO vehicle and could potentially operate up to Mach 15 (13: 3-4).

The typical dual flow path turbine based combination engine is the turboramjet engine. This engine features a single inlet within a single engine case, with separate internal flow-paths for the turbine engine and ram/scram engine. There are three distinct turboramjet operating modes, as detailed in Figure 9. The turbojet engine propels the vehicle from liftoff to Mach 0.9, while the ramjet inlet is closed. Then the ramjet inlet opens and turboramjet engine operates in dual mode until Mach 2.9, the upper bound for turbojet operation. At Mach 2.9 the turbojet engine inlet is closed and the engine is deactivated with subsequent ramjet operation only (17: 18). There are numerous variations of this engine to include turboscramjets that operate at even higher Mach numbers.

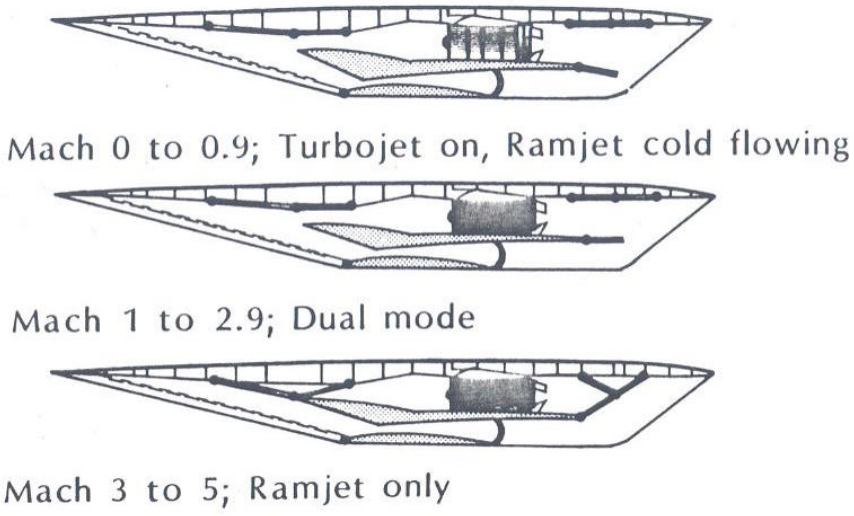

Figure 9: Turboramjet Operation Modes (17: 18)

The most complex TBCC engine, with a single flow-path, is typified by Mardquart's Mach 8 Supercharged Ejector Ramjet (SERJ) as shown in Figure 10. This conceptual engine operates at takeoff as an air-augmented rocket using the turbine assembly as a supercharger to further compress the incoming flow. The turbine's supercharging capability allows transition to ramjet operations at lower flight Mach numbers thus increasing engine efficiency. The turbine assembly can operate in an un-powered, wind-milling mode with minimal pressure losses up to Mach 6. The engine inlet temperatures reach 2500 ^{o}F and greater at flight conditions above Mach 6. These high temperatures will damage even advanced high temperature turbine blade materials or actively cooled turbines. The SERJ engine avoids this complication by physically removing the turbine assembly from the flow path, as shown in Figure 12, and continuing operation as pure ramjet. Escher believes that any airbreathing rocket engine will benefit from this supercharging turbine effect, including the Supercharged Ejector Scramjet (SESJ) engine that can operate up to Mach 15 (13: 3-11).

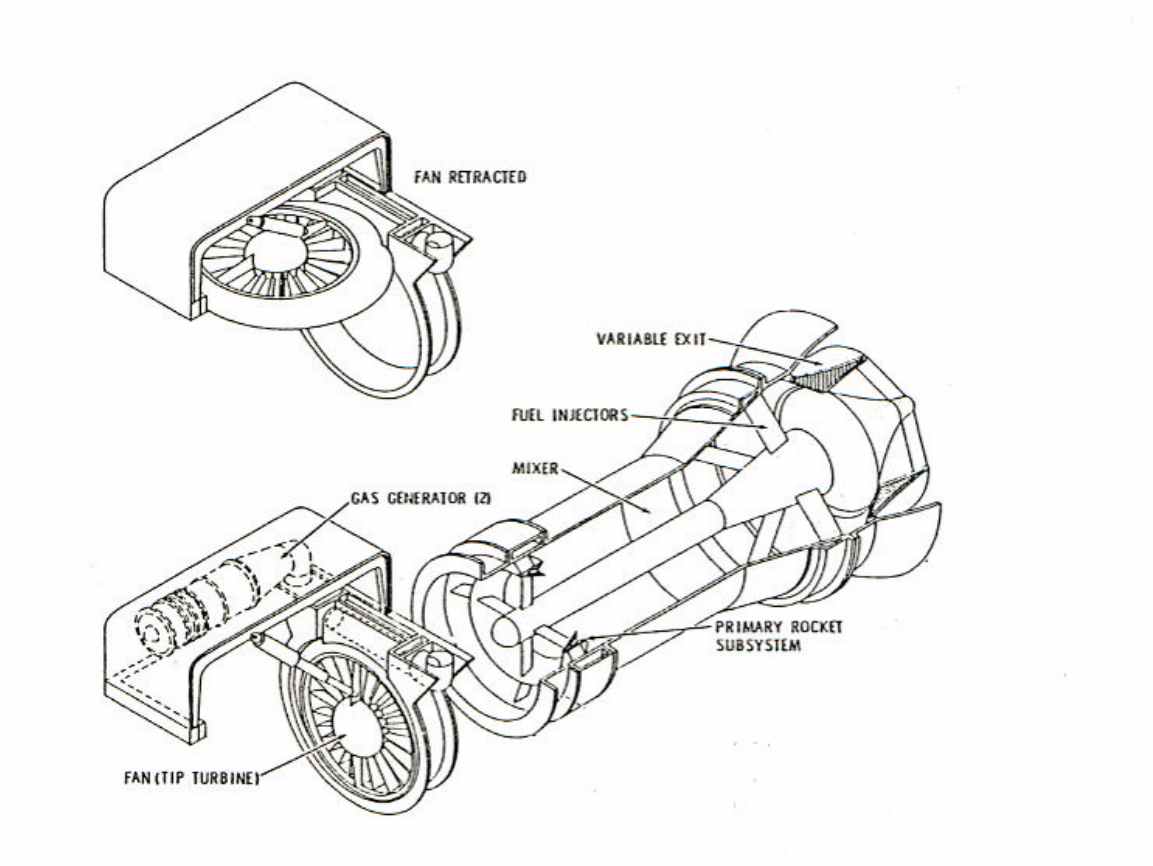

Figure 10: Supercharged Ejector Ramjet Engine (14: 9)

3. Methodology

A methodology was created to determine RLV performance. This method used theoretical RLV inert mass fractions to model vehicle stage weights. A GTOW was assumed for all RLVs studied and each vehicle's performance was based on two figures of merit: payload capacity to low Earth orbit and total inert weight. These two figures of merit were chosen because there is some contention amongst RLV researchers over which figure of merit is most influential to reducing RLV costs and thus improving performance. The two opposing views contend that either reductions in inert weight or increases in payload weight are most important to reduce costs (4: 1; 16: 3; 21:7; 31).

NASA's trajectory optimization program, Program to Optimize Simulated Trajectories (POST), was used as integral part of this method to simulate the RLV flight paths. RLV configurations were created based on assumptions detailed later.

Additionally, a sensitivity analysis of numerous trajectory constraints was conducted to determine the ideal launch trajectory of each RLV. The ideal launch trajectory defined as the trajectory that yields the maximum payload capacity. The ideal launch trajectories were then used to compare the performance of the 5 APTSS RLV's. Selected results were verified using a variant of the ideal rocket equation.

This chapter covers the method created to determine RLV stage weights, the sensitivity analysis technique, and technique to compare RLV performance. The following also details the

flight fundamentals, trajectory simulation program, the assumptions and figures of merit, and the specific vehicle configurations used in this study.

3.1 Flight Fundamentals

The RLVs studied in this research all utilized a lifting body aerodynamic shape that differs greatly from the typical expendable launch vehicle cylindrical fuselage. The aerodynamics of the vehicle behaves like any traditional airplane where the basic forces acting on the wings are lift (L), drag (D), weight (W), and thrust (T), all measured in pounds-force (lbf). The vehicle weight changes with time and is a function of propellant mass flow rate and weight reductions due to staging. Thrust is derived from engine capabilities and will be described in a subsequent section (1: 20). Lift and drag are governed by the following equations:

$$L = \frac{1}{2} \rho u^2 C_L S \qquad (1)$$

$$D = \frac{1}{2} \rho u^2 C_D S \qquad (2)$$

3.1.1 Rocket Propulsion Fundamentals

Rocket engine performance is defined by thrust and Isp. Rocket thrust, in lbf, is governed by the equation (18: 471)

$$T = \frac{\dot{m} u_e}{g_e} + \left(p_e - p_a \right) A_e \qquad (3)$$

Rocket Isp, in seconds, is given by (18: 471-472)

$$Isp = \frac{u_{eq}}{g_e} \qquad (4)$$

where

$$u_{eq} = u_e + \frac{g_e \left(p_e - p_a \right) A_e}{\dot{m}} \qquad (5)$$

3.1.2 Airbreathing Propulsion Fundamentals

Ideal airbreathing engine performance is defined by uninstalled engine thrust and specific fuel consumption or Isp. Uninstalled thrust, in lbf, is given by (18: 148)

$$T = \frac{(\dot{m} u_e - \dot{m}_a u)}{g_e} + \left(p_e - p_a \right) A_e \qquad (6)$$

Specific fuel consumption, SFC, in pound mass per second per pound force, is given by (17: 110)

$$SFC = \frac{\dot{m}_f}{T} \qquad (7)$$

Airbreathing engine Isp, in seconds, is given by (17: 111)

$$Isp = \frac{T}{\dot{m}_f} \qquad (8)$$

3.2 Program to Optimize Simulated Trajectories (POST)

POST, a 3 degree of freedom trajectory optimization program, was utilized to model the TSTO RLV trajectories. The program, created by NASA and Martin Marietta in the 1970s to model the Space Shuttle launch and landing trajectories, is an industry standard for optimizing vehicle trajectories. It is a generalized event-oriented Fortran 77 computer code that numerically integrates the equations of motion. POST allows the user to optimize the vehicle trajectory, based on a maximization or minimization of a number of vehicle properties, by varying flight trajectory and engine thrust. The program requires numerous inputs regarding vehicle performance and aerodynamic properties to include: lift coefficient and drag coefficient, engine thrust, and engine Isp. The user must provide guidance inputs such as staging conditions, takeoff velocity and location, dynamic pressure limitations, final on-orbit conditions, and many others. The program provides a detailed output file which indicates if the trajectory succeeded or failed to converge. The output file also provides a user-designated, time-interval display of over 100 flight variables. Up to 30 of these output variables can be imported into a Microsoft Excel spreadsheet format for easy use (27).

3.3 Aerospace Propulsion Technology Screening Study TSTO Configurations

The APTSS TSTO configurations were provided by AFRL's Propulsion Directorate, shown in Table 1. All RLVs are unmanned vehicles deemed capable of development within the next 10 years. Table 1 details the TSTO configuration ID, the propulsion method for vehicle stage, the takeoff method, and the ascent trajectory. All vehicles were launched into a 50 x 100 mile polar orbit. Fuels were restricted to hydrocarbon propellants like RP-1 and JP-7, while either liquid oxygen (LOx) or air was suitable oxidizer (31).

Table 1: APTSS RLV Configurations (31)

RLV ID	Flight Mode	Operating Mode	1st Stage Cycle	2nd Stage Cycle
Rkt-Rkt	Direct Ascent	Vertical Takeoff	Rocket	Rocket
Rkt-RBCC	Direct Ascent	Vertical Takeoff	Rocket	RBCC
TJ-Rkt1	Lifting Ascent	Horizontal Takeoff	Mach 4 Turbojet	Rocket
RBCC-Rkt	Direct Ascent	Vertical Takeoff	Mach 0-8 RBCC	Rocket
TJ-Rkt2	Lifting Ascent	Vertical Takeoff	Mach 4 Turbojet	Rocket

3.4 RLV Analysis Technique

The RLV analysis methodology shown below used POST in an iterative manner to determine breakdown of each RLV's stage weights. These stage weights included: inert weight, propellant weight, and payload weight. Using the assumed GTOW and stage mass fractions, the RLV payload capability and total inert weight were 'backed-out' from POST's output. The GTOW and RLV fuel weight were set equal, modeling the entire vehicle as fuel, and the inert masses and payload masses were extracted by running POST twice. The step by step process is described below.

-- Step 1: The vehicle GTOW and vehicle propellant weight of the entire RLV was set to 1,000,000 lbf.

-- Step 2: POST was run, and the staging condition vehicle weight (W_{stg}), in lbf, was taken directly from the first POST output file.

-- Step 3: The 1st stage propellant weight (W_{prop1}), in lbf, was determined by

$$W_{prop1} = GTOW - W_{stg} \qquad (9)$$

-- Step 4: Using the assumed 1st stage mass fraction (F_1), the 1st stage total weight (W_{tot1}), in lbf, was found by

$$W_{tot1} = \frac{W_{prop1}}{(1 - F_1)} \qquad (10)$$

The 1st stage total weight was defined as

$$W_{tot1} \equiv W_{prop1} + W_{inert1} \qquad (11)$$

where W_{inert1}, in lbf, was the 1st stage inert weight. F_1 was assumed based on data collected in the literature review, and was defined as

$$F_1 \equiv \frac{W_{inert1}}{W_{inet1} + W_{prop1}} \qquad (12)$$

Since the weight data collected for F_1 was given in pounds mass or in pounds-force at sea level, where 1lbm equals 1 lbf, it was acceptable to use the term 'inert mass fraction'. The selection of F_1 for each RLV configuration is discussed in a subsequent section.

-- Step 5: W_{inert1} was given by

$$W_{inert1} = W_{tot1} - W_{prop1} \qquad (13)$$

-- Step 6: The 2nd stage initial weight ($W_{initial2}$), in lbf, was determined by

$$W_{initial2} = W_{stg} - W_{inert1} \qquad (14)$$

The 2nd stage initial weight included the 2nd stage propellant, 2nd stage inert weight, and payload weight. This value was input into POST. The 2nd stage propellant weight, also input into POST, was set equal to $W_{initial2}$, modeling the entire 2nd stage as propellant.

-- Step 7: POST was run a second time, and the remaining propellant weight at orbit insertion (W_{orbit}), in lbf, was retrieved from POST's output.

-- Step 8: W_{orbit} was used to determine the 2nd stage propellant weight (W_{prop2}) by

$$W_{prop2} = W_{initial2} - W_{orbit} \qquad (15)$$

-- Step 9: Using the assumed 2nd stage mass fraction (F_2), the 2nd stage total weight (W_{tot2}), in lbf, was found by

$$W_{tot2} = \frac{W_{prop2}}{(1 - F_2)} \qquad (16)$$

The 2nd stage total weight was defined as

$$W_{tot2} \equiv W_{prop2} + W_{inert2} \qquad (17)$$

where W_{inert2}, in lbf, was the 2nd stage inert weight. F_2 was assumed based on data collected in the literature review, and is defined as

$$F_2 \equiv \frac{W_{inert2}}{W_{inet2} + W_{prop2}} \quad (18)$$

The selection of F_2 for each RLV configuration is discussed in a subsequent section.

-- Step 10: Using F_2, W_{inert2} was determined by

$$W_{inert2} = W_{tot2} F_2 \quad (19)$$

-- Step 11: Finally, the available payload weight (W_{pay}), in lbf, was found by

$$W_{pay} = W_{orbit} - W_{inert2} \quad (20)$$

An example of the output from this process for the Rkt-Rkt vehicle is shown in Table 2. In this example, both F_1 and F_2 were assumed to be 0.1.

Table 2: Rkt-Rkt Sample Weight Breakdown via POST Analysis

GTOW (lbf)	1000000
W_{stg} (lbf)	540366
W_{prop1} (lbf)	459634
W_{tot1} (lbf)	510704
W_{inert1} (lbf)	51070
$W_{initial2}$ (lbf)	489295
W_{tot2} (lbf)	471727
W_{inert2} (lbf)	47172
W_{orbit} (lbf)	64741
W_{prop2} (lbf)	424554
W_{pay} (lbf)	17568

3.4.1. Methods to Verify Results

A variation of the ideal rocket equation was used to verify the accuracy of the process described above. Since the ideal rocket equation applies for launch vehicles with rocket

engines, it was used only to verify the accuracy of results of the Rkt-Rkt RLV. Equation (21), which ignores drag forces and approximates the effects of gravity, was re-arranged into Equation (22) to determine payload and inert weight per stage based on the burn time, flight path angle, Isp values, and provided in the POST output (18: 474).

$$\Delta V = Isp_a g_e \ln(\frac{W_o}{W_b}) - g_e[\cos(q)]_{ave} t_b \qquad (21)$$

$$W_b = \frac{W_o}{\exp(\frac{\Delta V + g_e[\cos(q)]_{ave} t_b}{Isp_a g_e})} \qquad (22)$$

The step-by-step process for determining the payload weight via the rocket equation is shown below.

-- Step 1: Equation (22) was solved for W_{stg}, where W_o was set equal to the GTOW of 1,000,000 lbf and the other variables were taken from the POST output file. This yielded the following equation:

$$W_{stg} = \frac{GTOW}{\exp(\frac{\Delta V + g_e[\cos(q)]_{ave} t_b}{Isp_a g_e})} \qquad (23)$$

-- Step 2: W_{prop1} was determined by

$$W_{prop1} = GTOW - W_{stg} \qquad (24)$$

-- Step 3: Using the assumed F_1, the W_{tot1} was found by

$$W_{tot1} = \frac{W_{prop1}}{(1 - F_1)} \qquad (25)$$

F_1 was the same value used in the POST analysis.

-- Step 4: W_{inert1}, was given by

$$W_{inert1} = W_{tot1} - W_{prop1} \quad (26)$$

-- Step 5: $W_{initial2}$ was determined by

$$W_{initial2} = W_{stg} - W_{inert1} \quad (27)$$

-- Step 6: Equation (18) was solved for W_{orbit}, where W_o was set equal to $W_{initial2}$ and the other variables were taken from the POST output file. This yielded the following equation:

$$W_{orbit} = \frac{W_{initial2}}{\exp(\frac{\Delta V + g_e[\cos(q)]_{ave} t_b}{Isp_a g_e})} \quad (28)$$

-- Step 7: W_{orbit} was used to determine W_{prop2} via

$$W_{prop2} = W_{initial2} - W_{orbit} \quad (29)$$

-- Step 8: Using F_2, W_{tot2} was found by

$$W_{tot2} = \frac{W_{prop2}}{(1 - F_2)} \quad (30)$$

F_2 was the same value used in the POST analysis.

-- Step 9: Using F_2, W_{inert2} was determined by

$$W_{inert2} = W_{initial2} F_2 \quad (31)$$

-- Step 10: Finally, W_{pay}, was found by

$$W_{pay} = W_{orbit} - W_{inert2} \quad (32)$$

The payload weights determined by the rocket analysis and via POST were then compared. Since the rocket equation analysis did not account for drag, it was expected that

payload weights from that method should exceed those output by POST. An example of the output from the rocket equation analysis for the Rkt-Rkt vehicle is shown in Table 3.

Table 3: Rkt-Rkt Sample Weight Breakdown via Rocket Analysis

First stage	
?V (ft/sec)	1931
G (ft/sec^2)	32.2
$[\cos(?)]_{ave}$	0.89243
Isp_{ag} (ft/sec)	11914
GTOW (lbf)	1000000
t_b (sec)	91
W_{stg} (lbf)	682790
F_1	0.1
W_{prop1} (lbf)	317209
W_{tot1} (lbf)	352455
W_{inert1} (lbf)	35245
Second Stage	
?V (ft/sec)	22653
G (ft/sec^2)	32.2
$[\cos(?)]_{ave}$	0.166057
Isp_{ag} (ft/sec)	11914
$W_{initial2}$ (lbf)	647544
F_2	0.1
t_b (sec)	238
W_{orbit} (lbf)	86920
W_{prop2} (lbf)	560623
W_{inert2} (lbf)	64754
W_{pay} (lbf)	22146

In order to further verify the accuracy of POST, a single Rkt-Rkt POST run was conducted with the lift and drag of the vehicle 'turned off' in the input file. This allowed a straight comparison between the rocket equation analysis and the POST output. This analysis is shown in the results section.

The accuracy of POST's weight results for the other vehicles in this study could not be verified using the rocket equation method shown above, thus a different technique was used. The engine thrust displayed in the POST output file was checked against the engine data. This check was performed at various flight altitudes and Mach numbers. This verification was deemed sufficient because the verification of the Rkt-Rkt method proved that the proposed methodology using POST was accurate.

3.5 Assumptions

A comprehensive literature review of RLV designs similar to those in the APTSS guidance was conducted to base the assumptions for the study. This prevented the time consuming, and almost impossible task of designing 5 different RLVs. Assumptions were made regarding vehicle mass properties, aerodynamic properties, engine configuration and performance capabilities, and flight trajectory. These assumptions served as the baseline for each vehicle configuration.

3.5.1 Vehicle Mass Properties

The primary assumption for the RLV analysis was vehicle GTOW and stage inert mass fractions. The study assumed all vehicles had a GTOW of 1,000,000 lbf. Although this weight is not large when compared to some expendable launch vehicle weights, it was chosen because most established airport runways can support an airplane of that magnitude, like a Boeing 747 (3: 3-4; 22: 20). This facilitates the operation of a horizontal takeoff RLV within the next 10 years, without any major change to existing infrastructure. Inert mass fraction data, detailed in

Table 4, was collected from RLV studies based on propulsion type per vehicle stage. Data was collected on turbojet, RBCC and rocket propelled vehicles.

Table 4: RLV Mass Fraction Data

TJ Stages	Reference	Inert Mass Fraction
	15	0.31
	15	0.42
RBCC Stages	**Reference**	**Inert Mass Fraction**
	11	0.23
	6	0.36
	6	0.37
	6	0.34
Rocket Stages	**Reference**	**Inert Mass Fraction**
	21	0.16
	21	0.12
	16	0.15
	16	0.08
	11	0.18
	6	0.26
	6	0.25
	6	0.25
	6	0.24
	6	0.25
	15	0.16
	17	0.22

Based on the data presented above, mass fractions for each baseline RLV configuration were selected as illustrated in Table 5. The turbojet and RBCC stage mass fractions were chosen because they were the mean value of those in Table 2. The mean rocket mass fraction was 0.17, but cursory analysis on the Rkt-Rkt RLV with this value yielded insufficient fuel to

reach orbit. A rocket mass fraction of 0.1 was used as a baseline value because it allowed the Rkt-Rkt vehicle to reach orbit with a nominal payload, and it fell within the range shown in Table 4. Superficial analysis also revealed that mass fraction much larger than 0.1 caused the baseline TJ-Rkt1 and TJ-Rkt2 vehicles to have insufficient fuel to reach orbit. Accordingly, rocket stages for all vehicles were assigned a mass fraction of 0.1.

Table 5: APTSS RLV Baseline Assumptions

APTSS RLV ID	**Rkt-Rkt**	**Rkt-RBCC**	**TJ-Rkt1**	**TJ-Rkt2**	**RBCC- Rkt**
Inert Mass Fraction					
1st stage	0.1	0.1	0.35	0.35	0.30
2nd stage	0.1	0.30	0.1	0.1	0.1
Staging Conditions					
Dynamic Pressure (lbf/ft^2)	350	350	350	350	350
Mach	3	4	N/A	N/A	8
Max Dynamic Pressure (lbf/ft^2)	600	600	2250	2250	2250
Drag Coefficient Multiplier	1	1	0.25	0.25	1
Axial g-load Limit	3.5	3.5	3.5	3.5	3.5
Horizontal Takeoff Velocity (ft/sec)	N/A	N/A	300	N/A	N/A
1st Stage Engine Configuration					
Type of Engine	RD-180	RD-180	Turbojet	Turbojet	RBCC (RD-180/scramjet)
Number of Engines	2	2	12	25	2 RD-180/ 1 scramjet
Inlet/Exit Area per engine (ft^2)	75.4	75.4	14/16.88	14/16.88	RD-180: 75.4 Scramjet: 400/140
2nd Stage Engine Configuration					
Type of Engine	RD-180	RBCC (RD-180/scramjet)	RD-180	RD-180	RD-180
Number of Engines	1	1	1	1	1
Inlet/Exit Area per engine (ft^2)	75.4	RD-180: 75.4 Scramjet: 400/140	75.4	75.4	75.4

3.5.2 Aerodynamic Properties

The POST input file for each RLV configuration required aerodynamic data detailing the vehicle's lifting surface area, and the lift and drag coefficients of the vehicle based on flight Mach number and angle of attack. This data was used by the program to determine lift and drag properties via Equations (1) and (2).

The wedge shaped X-43 lifting body vehicle was chosen as the baseline aerodynamic shape for both stages of the RLV configurations. The X-43 was chosen because its aerodynamics are well characterized and the vehicle has been built, thus providing realistic RLV aerodynamic properties. The X-43 lifting body configuration, with the underside air-frame integrated scramjet engine, is also consistent with many theoretical vehicles from the literature review (16: 6; 21: 3; 11: 9; 6: 1-2: 22: 8). The major limitation to using the X-43 data is that the airframe was designed for only for hypersonic speeds, and not low speed flight. Additionally, it is unlikely that any future vertical takeoff RLV that does not utilize a lifting ascent trajectory will have an airframe similar to the X-43. These vehicles would most resemble a modern day expendable launch vehicle fuselage. The X-43 aerodynamic properties are displayed in Appendix A (31). The drag coefficients of the TJ-Rkt1 and TJ-Rkt2 RLVs were reduced to 25 percent of the X-43 baseline value after cursory analysis found that the immense drag at low Mach numbers was prohibiting vehicle acceleration and altitude gain. The drag coefficient multipliers for all vehicles studied are shown in Table 5.

The vehicle lifting surface reference area was based on data from lifting body RLVs with GTOWs close to one million pounds. Although data was limited, a 1st stage lifting surface

reference area of 10500 ft^2 was selected for all the configurations based on the information displayed in Table 6. A 2nd stage lifting surface reference area of 2585 ft^2 was chosen based on common data set for both a one million pound TBCC and RBCC first stage TSTO RLV with a rocket second stage (6).

Table 6: Lifting Body Reference Areas

RLV GTOW (lbf)	Aerodynamic Reference Area (ft^2)	Engine Inlet Area (ft^2)	Reference
1,000,000	10500	340-628	6
1,000,000	N/A	400	14
1042786.5	11062	N/A	15

3.5.3 Engine Configuration and Performance

The POST input file for each RLV configuration required extensive engine performance data. Obtaining valid engine data became one of the largest obstacles to completing this research. Scramjet and turbojet data were provided by AFRL, while rocket data was derived from modern flight-ready engines. RBCC and scramrocket performance data were unavailable, and were approximated. Engines were conceptually attached to the aerodynamic reference body. Selected engine specifications for all RLVs studied are summarized in Table 5.

3.5.3.1 Rocket Engines

Rocket engine performance for all vehicles was modeled using vacuum Isp, vacuum thrust, and exit area data from the RD -180 engine. This RP-1 fueled engine was used as a baseline because of its current flight ready, reliable, status with the Atlas III and Atlas V launch

vehicles. At the direction of AFRL, the RD-180 engine Isp was increased to 370 from 337 seconds to simulate advances in rocket engine performance that may occur over the next 10 years (31). The standard RD-180 exit area of 75.4 ft^2 and vacuum thrust of 933,000 lbf were assumed (30). Two RD-180 engines were used for the first stages of the Rkt-Rkt, RBCC-Rkt, and Rkt-Scrkt1 RLVs. This provided sufficient thrust for vertical takeoff. One RD-180 engine was needed for each RLV second stage.

3.5.3.2 Scramjet Engines

Scramjet engine performance data for the HRE engine was provided by AFRL. The data, shown in Appendix B, was derived from the HRE engine, using JP-7 fuel. Given that the engine was designed and built in the 1960s, although never flight-tested, it is believed by AFRL that such an engine is technically feasible within 10 years. The engine deck provided uninstalled thrust coefficient and Isp data as a function of flight altitude and Mach number. The engine was 'sized up' by a factor of 64.5 to be consistent with underside body-integrated airbreathing engines from the literature review, as shown in Table 5 (31). This yielded an engine inlet area of 400 ft^2 and exit area of 140 ft^2.

3.5.3.3 Turbojet Engines

Turbojet engine performance data for the RLV configurations with turbojet first stage propulsion is provided by AFRL. The complete propulsion data, shown in Appendix B, was from AFRL's conceptual Mach 4 turbine accelerator design with a sea level thrust of 51,620 lbf. The engine deck provided uninstalled thrust and specific impulse information, for the JP-4

fueled engine, as a function of flight altitude and Mach number. The engine inlet area and exit area are 14 ft^2 and 16.88 ft^2, respectively (31).

Given the relatively low turbojet thrust, at least an order of magnitude less when compared to the RD-180 rocket engine, 25 turbojet engines were needed to lift the TJ-Rkt2 vehicle off the launch pad. These 25 engines provided a liftoff thrust to weight (T/W) ratio of 1.3/1. Furthermore, data from the literature review verified 1.3/1 to be a reasonable takeoff T/W ratio for a vertical takeoff launch vehicle (3: 5). Turbojet engine specifications for the TJ-Rkt2 vehicle are detailed in Table 5.

Multiple POST runs, using different numbers of turbojet engines, revealed 12 turbojet engines to be the minimum number needed for the TJ-Rkt1 RLV to overcome the excessive drag from the X-43 airframe at low Mach numbers. As seen in Figure 11, which plots the thrust and drag force from the baseline TJ-Rkt1 RLV configuration versus time after liftoff, the drag reached a maximum of almost 500,000 lbf early in flight. The excessive drag reduced the vehicle's acceleration and prolonged first stage flight. When using fewer than 12 turbojet engines, the engine thrust was insufficient to overcome this drag in order to accelerate to Mach 4. The takeoff T/W ratio of 12 engines was 0.67. This takeoff T/W ratio fell within the range of 0.5 to 0.7 which was indicated in the literature for horizontal takeoff RLVs (3: 4). Turbojet engine specifications for the TJ-Rkt1 are detailed in Table 5.

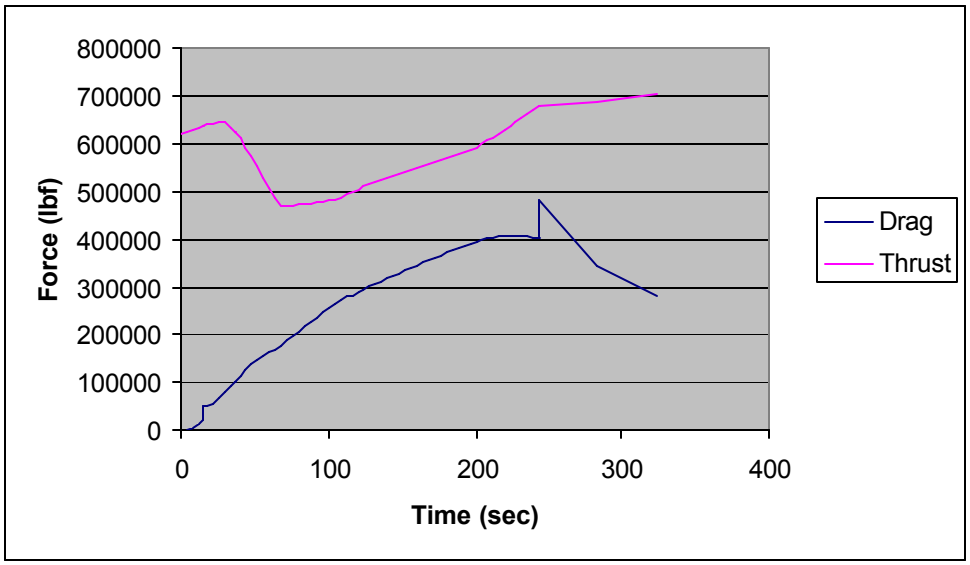

Figure 11: TJ-Rkt1 Thrust and Drag Force vs. Time

3.5.3.4 RBCC Engine

RBCC engine performance data was unavailable; therefore, engine data was modeled with the RD-180 and the HRE scramjet engine information. This technique, recommended by AFRL, modeled the RD-180 rocket as a secondary thrust chamber within HRE derived scramjet with a retractable inlet (31). This configuration was similar to the ESJ shown in Figures 7 and 8. Both sets of engine data were input into POST and the two engines operated simultaneously throughout operation. Ideally the RBCC engine would have been modeled using a higher Isp air-augmented rocket in place of the RD-180, but air-augmented rocket data was unavailable. This method ignored any performance losses due to engine integration. The RBCC engine was used for the 2nd stage engine of the Rkt-RBCC RLV and for the 1st stage engine of the RBCC-Rkt RLV, as shown in Table 5.

3.5.4 Flight Trajectory Assumptions

Each POST input file required a small number of trajectory assumptions. The majority of these assumptions varied per RLV configuration and was derived from data in the literature review. Horizontal takeoff speed, launch-site, staging dynamic pressure, maximum g-limit, and maximum dynamic pressure were assumed for the study. The trajectory constraints were repeatedly found in the RLV literature.

3.5.4.1 Horizontal Takeoff Speed and Launch Site

The Vandenberg AFB launch site was chosen for all launches. The only two sites considered for were Vandenberg AFB, CA and Cape Canaveral, FL. Both sites had established infrastructure for both vertical and horizontal takeoff vehicles. Vandenberg AFB was chosen as the launch site for this study.

The literature review found that a horizontal takeoff velocity range of 229 – 320 ft/sec was theorized in RLV conceptual designs (4: 7; 21: 3). A horizontal takeoff velocity of 300 ft/sec was chosen for all horizontal takeoff APTSS configurations.

3.5.4.2 Dynamic Pressure Assumptions

Dynamic pressures throughout a launch trajectory exert structural and aero-heating loading on the launch vehicle. Vehicles must be designed to withstand these dynamic pressure loadings or the vehicle trajectory must be tailored to reduce dynamic pressure along the ascent. More robust vehicles, with larger mass fractions like those propelled by airbreathing engines, can withstand greater dynamic pressure loadings.

More fragile structures like rockets withstand far lesser loads from dynamic pressure (4: 4). Dynamic pressure limits assumed for all vehicles in this study are displayed in Table 5.

According to multiple sources the dynamic pressure range for airbreathing propelled RLVs was found to be from 1500- 2250 lbf/ft^2 (22; 4; 6; 11). Typically, airbreathing engines provide more thrust at greater dynamic pressures. The RLVs typically reached this dynamic pressure quickly then accelerated along a line of constant dynamic pressure until shortly before staging. Cursory POST runs of the TJ-Rkt1 RLV configuration revealed that there was insufficient thrust to overcome gravity and drag when operating the 12 AFRL turbojet engines at maximum dynamic pressures less than 2250 lbf/ft^2. The TJ-Rkt2 vehicle did not encounter problems overcoming drag due the immense thrust from its 25 turbojet engines, but the RLV's maximum dynamic pressure was also constrained to 2250 lbf/ft^2 to maintain consistency with the TJ-Rkt1 vehicle. This consistency aided in comparing the two vehicle's performance.

The scramjet mode of the RBCC engines used by the RBCC-Rkt and Rkt-RBCC, RLVs were constrained to a maximum dynamic pressure of 2250 lbf/ft^2. This dynamic pressure loading was chosen to maintain consistency with the turbojet vehicle configuration.

There was an abundance of data regarding dynamic pressure limitations on rockets in general. Unfortunately, only one source of RLV rocket data was found, and it indicated a maximum dynamic pressure of 500 lbf/ft^2 (4). Fortunately, extensive expendable rocket data was found, as shown in Table 7. A dynamic pressure limitation of 600 lbf/ft^2 was placed on all

RLV rocket stages in the study. This low number was chosen because it was within the range of all the data collected, but it was closer to the only source of RLV data.

Table 7: Expendable Launch Vehicle Maximum Dynamic Pressure and Maximum g-Loading (20)

Vehicle Type	Max Axial g's	Max Dynamic Pressure (lbf/ft^2)
Atlas	6	700-800
Delta	3.75-6	890-2150
Titan 4	5	975
Zenit	4.5	1080
Soyuz	4	N/A
Proton	4.3	800
Kosmos	6.9	1100

Staging dynamic pressure limitations were found in several literary sources to range from 200 – 350 lbf/ft^2 (21; 6; 11). All vehicles in the literature review 'pitched-up' along their trajectories prior to staging to reduce the dynamic pressure and thus the loading on the vehicle during the staging. The upper bound dynamic pressure of 350 lbf/ft^2 was chosen as the baseline staging point for all RLV configurations due to optimization difficulties experienced with the TJ-Rkt1 configuration when using the lower values. This problem will be discussed in more detail in the results section. All other RLV configurations were assigned the same staging dynamic pressure to ensure consistency. Each RLV's staging dynamic pressure limit is shown in Table 5.

3.5.4.3 Maximum Axial g-limit

A maximum axial g-loading was assumed for both stages of all RLV configurations. The g-limit data collected on expendable rockets is shown in Table 7. RLV g-limit data was sparse, but both sources indicated a max load of 3g's (4; 21). Based on this information a maximum 3.5g limit was chosen. This maximum g-loading fell well within the ranges published for both RLVs and expendable launch vehicles, but was closer to the RLV data.

3.5.4.4 Staging Mach Number

Baseline staging Mach numbers were selected for the Rkt-Rkt, RBCC-Rkt and Rkt-RBCC RLV configurations. Based on recommendations from AFRL, due to an absence of published data, a baseline staging Mach number of 3 was chosen for the Rkt-Rkt vehicle. A Mach 4 staging condition was assumed for the Rkt-RBCC to utilize the full operating envelope of the scramjet mode of the 2nd stage RBCC engine. A Mach 8 staging condition was assumed for the RBCC-Rkt to utilize the full operating envelope of the scramjet mode of the 1st stage RBCC engine. (31).

The TJ-Rkt1 and TJ-Rkt2 RLVs did not have a staging Mach number. The first stages of both vehicles accelerated along a constant dynamic pressure line of 2250 lbf/ft^2 until they reached Mach 4. At Mach 4, they 'pitched-up' to reduce the dynamic pressure to the staging dynamic pressure of 350 lbf/ft^2. During this pitch-up maneuver both vehicles lost velocity and staged at a Mach number less than Mach 4. Staging conditions for all RLVs studied are shown in Table 5.

3.6 Sensitivity Analysis

A sensitivity analysis was performed on the trajectory constraints for the Rkt-Rkt RLV. One trajectory constraint was varied over the range found in the literature review, while the others were held constant. The effects of variations in staging dynamic pressure, maximum dynamic pressure, maximum g-loading, and staging Mach number were studied.

The effect of drag coefficient variations on vehicle performance was studied on the Rkt-Rkt vehicle as well. The drag coefficients were varied, in the POST input file, from the X-43 baseline down to 25 percent of that value. This study was done because the X-43 vehicle aerodynamics were quite dissimilar from any future proposed RLV like the Rkt-Rkt. The 25 percent drag coefficient value was then used in Rkt-Rkt optimal launch trajectory to determine the Rkt-Rkt RLV's performance. This was done to maintain consistency amongst all the vehicles studied in the performance analysis.

Rocket Isp was varied from the actual RD-180 Isp value of 340 seconds up to 400 seconds. This range represented approximately a plus or minus 8 percent performance variation from the AFRL selected baseline of 370 seconds. This allowed for plausible increases or stagnation in rocket engine performance over 10 years (31). The lower Isp bound of 340 seconds was chosen to examine how the RLV performance would be affected if the Isp of the modern RD-180 did not improve in the next 10 years.

Sensitivity analyses were not performed on other RLV configurations. The problems that prevented sensitivity analyses on the other RLVs are explained in the results section.

3.7 Performance Analysis

An inert mass fraction analysis was conducted on the RLVs, based on the assumptions listed in Table 5, to compare each vehicle's performance. The Rkt-Rkt RLV's performance was studied using the ideal trajectory found via the sensitivity analysis, instead of using the assumptions listed in Table 5. Each RLV's stage inert mass fractions were varied over the ranges found in the literature review to determine available payload weight and inert weight. For the RLVs with dissimilar stage types, like the TJ-Rkt1 vehicle, the turbojet stage mass fraction was varied independently of the rocket stage mass fraction. This provided two separate mass fraction analyses for each vehicle of this type. Both stage mass fractions for the Rkt-Rkt configuration were varied simultaneously. This process provided a detailed examination of which stage mass fractions were most influential on vehicle performance.

4. Results

4.1 APTSS RLV Analysis

4.1.1 Rkt-Rkt Configuration

The results from the numerous sensitivity analyses on the Rkt-Rkt RLV, vertical takeoff, direct-ascent, RLV are shown below. Selected data is shown in this section, while full weight data is provided in Appendix C. The baseline trajectory and propulsion configuration used for all sensitivity analyses on the Rkt-Rkt RLV are detailed in Table 5.

4.1.1.1 Rkt-Rkt Configuration Aerodynamics Sensitivity

The aerodynamic sensitivity analysis via POST revealed that the available payload weight varies slightly with drag coefficient. The available payload weight increased as drag coefficient decreased, as shown in Table 8. This was expected because the retarding force of drag caused the RLV to expend more propellant to overcome increasing drag. This increase in required propellant directly resulted in less payload weight lifted to orbit. The effect of drag coefficient on payload weight was not severe, as shown in Figure 12. When the X-43 drag coefficient was set to zero, the RLV lifted 8.4% more payload weight to orbit when compared to the RLV with the unaltered X-43 drag coefficient. This shows that the aerodynamics of the direct ascent vehicle did not have a major influence on the RLV's performance. This relative insensitivity to drag coefficient validated the use of X-43 aerodynamic data for the vertical takeoff, direct ascent Rkt-Rkt configuration.

Table 8: Rkt-Rkt Aerodynamic Analyses Trajectory and Mass Data

Percent of X-43 Cd	**0**	**0.25**	**0.5**	**0.75**	**Baseline**
Rocket Equation Output					
First stage					
?V (ft/sec)	1931	1931	1931	1931	1931
$[\cos(?)]_{ave}$	0.909586	0.912254	0.907401	0.904841	0.89243
burn time (sec)	85.7	86.3	87.5	89.4	92
Second Stage					
?V (ft/sec)	22653	22653	22653	22653	22653
$[\cos(?)]_{ave}$	0.160467	0.180637	0.179314	0.173328	0.166057
burn time (sec)	253	245	245	242	239
Wpay (lbf)	22121	21227	21257	21620	22146
POST Output					
Wpay (lbf)	19038	19012	18810	18161	17568
Difference between payload weights	3083	2214	2447	3458	4578

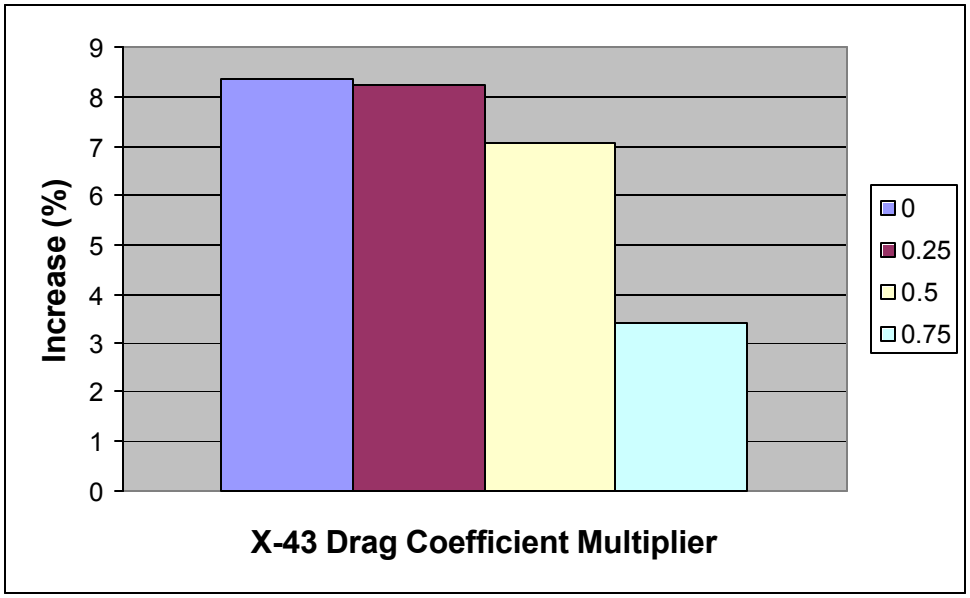

Figure 12: Percent Increase in Payload Weight above Baseline Payload Weight vs. X-43 Cd Multiplier for Rkt-Rkt RLV

While POST's results indicated that payload weight depended on drag coefficient multiplier, the rocket analysis indicated otherwise. As shown in Table 8, the payload weights determined via the rocket analyses were unaffected by drag coefficient. This was plausible because the variant of rocket equation used, Equation (22), did not account for drag force. Payload weight results from Equation (22) depended solely on burn times, ? Vs, and flight path angles of the RLV. As shown in Table 8, these quantities did not change considerably as the drag coefficient multiplier changes.

The results from the rocket equation did verify the accuracy of POST's results. As expected, the payload weights via the rocket analysis were considerably more than those found using POST. The difference, shown in Table 8, was sensible, considering that the rocket equation ignored retarding forces and used an average Isp and cos(?) values.

4.1.1.2 Rkt-Rkt Configuration Staging Dynamic Pressure Sensitivity

The staging dynamic pressure sensitivity analysis via POST yielded a clear trend. The payload weight available decreased with decreasing staging dynamic pressure as shown in Table 9. The staging dynamic pressure was varied from 350 lbf/ft^2 down to 220 lbf/ft^2. The POST trajectory failed to converge at dynamic pressures less than 220 lbf/ft^2. As shown in Figure 13, small variations in staging dynamic pressure, down to values of 280 lbf/ft^2, had little effect on payload weight. The effect on payload weight became more pronounced in the range from 260 lbf/ft^2 down to 220 lbf/ft^2. The payload weight for the 220 lbf/ft^2 case was 13.6% less than the baseline case's payload weight.

Table 9: Trajectory and Mass Data from the Rkt-Rkt Staging Dynamic Pressure Analyses

Staging Dynamic Pressure (lbf/ft^2)	**Baseline**	**325**	**300**	**280**	**260**	**240**	**220**
Rocket Equation Output							
First stage							
?V (ft/sec)	1931	1934	1937	1940	1942	1945	1976
$[\cos(?)]_{ave}$	0.89243	0.89949	0.90708	0.91402	0.92313	0.93162	0.82451
burn time (sec)	91	91.3	91.5	91.5	91.8	91.8	110
Second Stage							
?V (ft/sec)	22653	22651	22648	22645	22641	22639	22608
$[\cos(?)]_{ave}$	0.16605	0.16871	0.16367	0.16871	0.17069	0.16511	0.16511
burn time (sec)	238.5	238	237.5	237.5	238	240	228
Wpay (lbf)	22146	22083	22330	22479	22939	23776	20873
POST Output							
Wpay (lbf)	17568	17553	17497	17363	16838	16106	15187
Difference between payload weights	4578	4529	4832	5116	6100	7669	5686

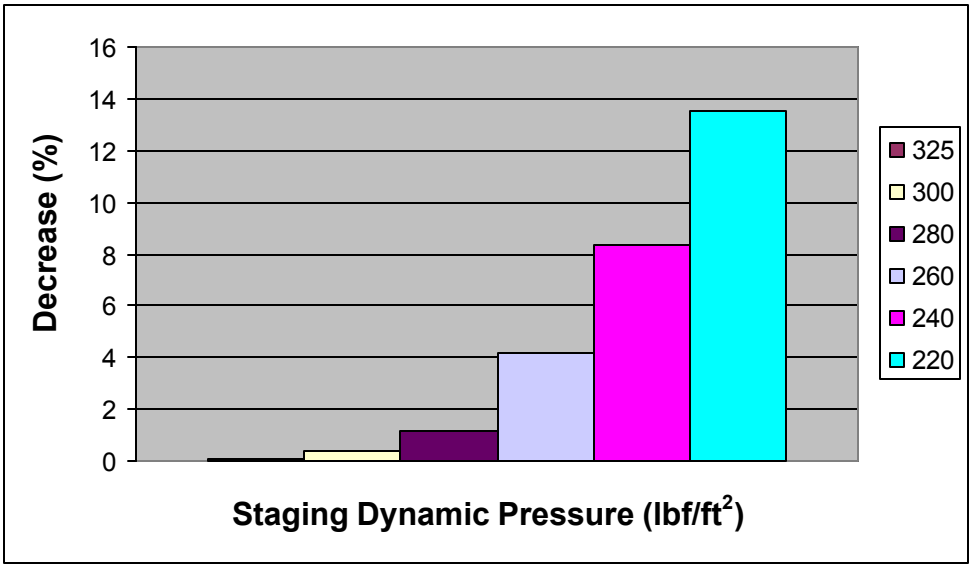

Figure 13: Percent Decrease in Payload Weight below Baseline Payload Weight vs. Staging Dynamic Pressure for Rkt-Rkt RLV

4.1.1.3 Rkt-Rkt Configuration Staging Mach Number Sensitivity

This analysis revealed that payload weight increased with increasing staging Mach number, as shown in Table 10. The staging Mach number was varied from 2.6 to 7.5 and an optimal Mach number of 7.0 was discovered. Mach numbers less than 2.6 were not investigated because the POST trajectory failed to converge at these values. The trajectories with staging Mach numbers greater than 7.0 yielded unorthodox flight paths which will be discussed in a subsequent section. The staging Mach number had a pronounced effect on payload weight as shown in Figure 14. The maximum payload weight, at a staging Mach number of 7, was 62% greater than the baseline configuration's payload weight.

The payload weights computed by the rocket analysis, as shown in Table 10, also increased with increasing staging Mach number. This trend was similar to the trend indicated by POST's output. This correlation validated POST's results.

Table 10: Trajectory and Mass Data from the Rkt-Rkt Staging Mach Number Analyses

Staging Mach Number	**Baseline**	**4**	**5**	**6**	**7**
Rocket Equation Output					
First stage					
?V (ft/sec)	1931	2864	3864	4906	5951
$[\cos(?)]_{ave}$	0.89243	0.85241	0.762738	0.716452	0.783573
burn time (sec)	91	103	113	123	136
Second Stage					
?V (ft/sec)	22653	21721	20721	19678	18629
$[\cos(?)]_{ave}$	0.166057	0.168717	0.163676	0.168719	0.170694
burn time (sec)	238.5	210	198	185	175
Wpay (lbf)	22146	27182	32092	35490	38726
POST Output					
Wpay (lbf)	17559	22855	26237	28191	28426
Difference between payload weights	4586	4327	5855	7299	10300

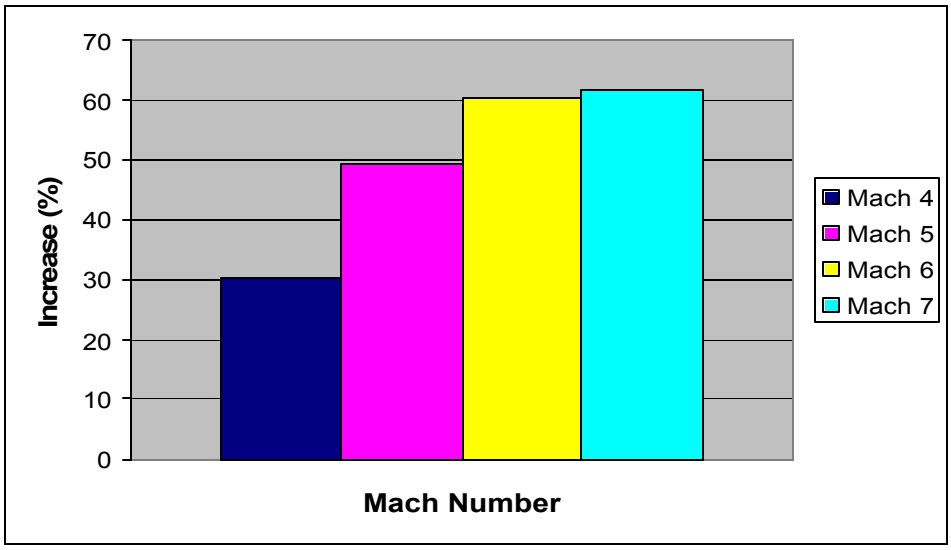

Figure 14: Percent Increase in Payload Weight above Baseline Payload Weight vs. Staging Mach Number for Rkt-Rkt RLV

4.1.1.4 Rkt-Rkt Configuration Maximum Dynamic Pressure Sensitivity

Examining the effects of maximum dynamic pressure proved to be the most difficult aspect of the Rkt-Rkt study. The maximum dynamic pressure was studied over a limited range from 600 lbf/ft^2 to 475 lbf/ft^2. Analysis outside that range was impossible because the POST trajectories failed to converge for trajectories with maximum dynamic pressures less than 475 lbf/ft^2 and greater than 600 lbf/ft^2.

The payload weights computed by POST were relatively independent of maximum dynamic pressure, as shown in Figure 15. Table 11 reveals that the payload weights predicted by the rocket analysis were also independent of maximum dynamic pressure. The accuracy of POST's payload weights was supported by the constant payload weight difference between the rocket analysis output and POST's output, as shown in Table 11.

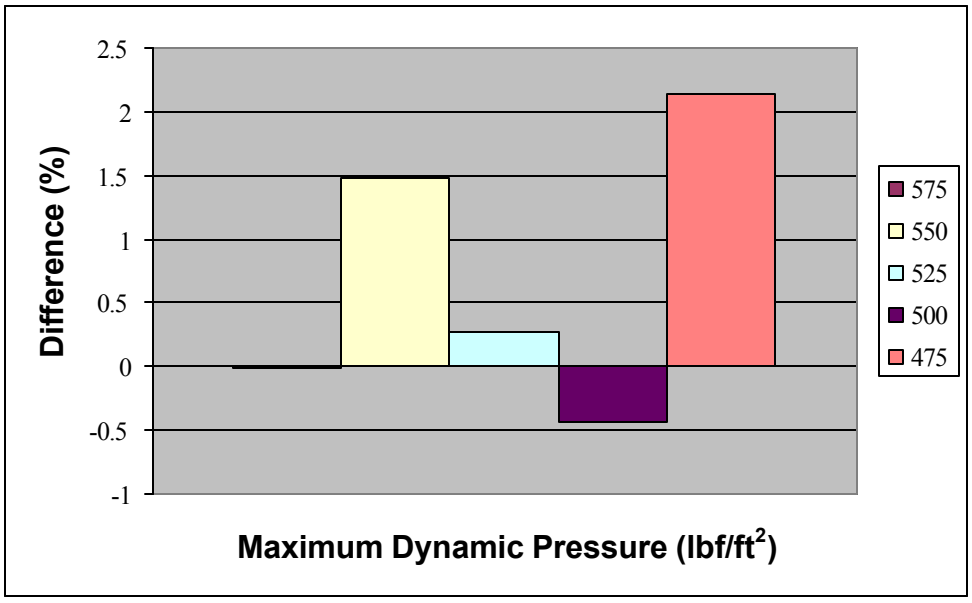

Figure 15: Percent Change in Payload Weight from Baseline Payload Weight vs. Maximum Dynamic Pressure for Rkt-Rkt RLV

Table 11: Trajectory and Mass Data from the Rkt-Rkt Maximum Dynamic Pressure Analyses

Maximum Dynamic Pressure (lbf/ft^2)	Baseline	575	550	525	500	475
Rocket Equation Output						
First stage						
?V (ft/sec)	1931	1931	1931	1931	1931	1931
$[\cos(?)]_{ave}$	0.89243	0.89779	0.89332	0.89556	0.89484	0.81767
burn time (sec)	91	91.4	92.3	92.6	93.5	104
Second Stage						
?V (ft/sec)	22653	22653	22655	22655	22653	22653
$[\cos(?)]_{ave}$	0.16605	0.16871	0.16367	0.16871	0.17069	0.16511
burn time (sec)	238	237.6	238.7	237.4	237.5	236
Wpay (lbf)	22146	21974	22170	21907	21757	22027
POST Output						
Wpay (lbf)	17559	17562	17300	17511	17636	17184
Difference between payload weights	4586	4412	4870	4395	4121	4842

4.1.1.5 Rkt-Rkt Configuration Maximum g-limit Sensitivity

The maximum g-loading on the Rkt-Rkt RLV had negligible impact on payload weight computed by POST, as shown in Table 12. The maximum g-limit was varied over the converged trajectory range of 3 g's through 6 g's. The largest payload weight was 0.24 percent above the baseline payload weight, as shown in Figure 16. As shown in Table 12, the rocket analysis also indicated that the maximum g-limit had little effect on payload weight. The correlation between POST's results and those obtained from the rocket equation further verifies the accuracy of POST's payload weights.

Table 12: Trajectory and Mass Data from the Rkt-Rkt Maximum g-limit Analyses

Maximum g-limit	**3**	**Baseline**	**4**	**4.5**	**5**	**5.5**	**6**
Rocket Equation Output							
First stage							
?V (ft/sec)	1931	1931	1931	1931	1931	1931	1931
$[\cos(?)]_{ave}$	0.89132	0.89243	0.89231	0.89275	0.89281	0.89284	0.89287
burn time (sec)	91.1	91	91	91	91	91	91
Second Stage							
?V (ft/sec)	22653	22653	22655	22655	22655	22655	22655
$[\cos(?)]_{ave}$	0.16215	0.16605	0.17672	0.18277	0.18799	0.19247	0.19674
burn time (sec)	264	238	220	208	199	192	187
Wpay (lbf)	21398	22146	22303	22503	22646	22753	22792
POST Output							
Wpay (lbf)	17406	17558	17602	17526	17456	17399	17355
Difference between payload weights	3991	4588	4701	4977	5190	5354	5437

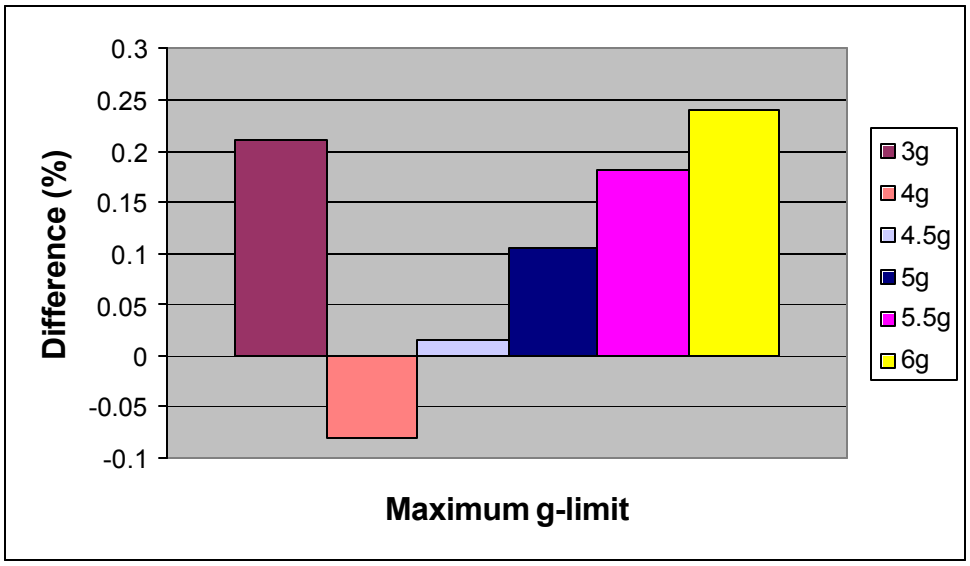

Figure 16: Percent Change in Payload Weight from Baseline Payload Weight vs. Maximum g-limit for Rkt-Rkt RLV

4.1.1.6 Rkt-Rkt Configuration Isp Sensitivity

The payload weight computed by POST dropped significantly with decreasing Isp, as shown in Figure 17. This phenomenon was expected because lower Isp values result in lower engine efficiency. Additionally, POST's payload weights were validated because the rocket analysis payload weights followed the same trend, as shown in Table 13.

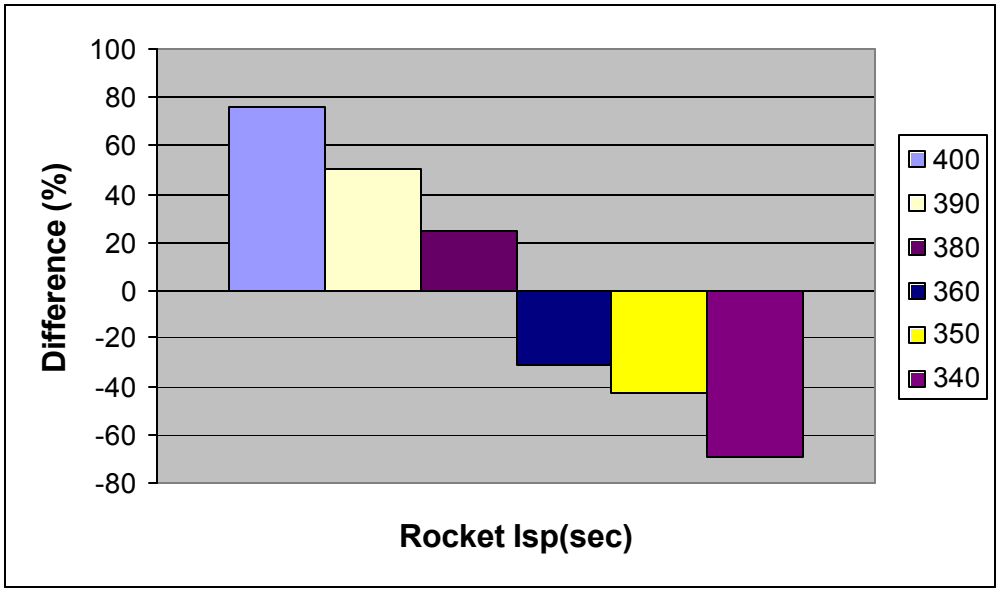

Figure 17: Percent Change in Payload Weight from Baseline Payload Weight vs. Rocket Isp for Rkt-Rkt RLV

Table 13: Trajectory and Mass Data from the Rkt-Rkt Rocket Isp Analyses

Rocket ISP (sec)	**400**	**390**	**380**	**Baseline**	**360**	**350**	**340**
Rocket Equation Output							
First stage							
?V (ft/sec)	1931	1931	1931	1931	1931	1931	1931
$[\cos(?)]_{ave}$	0.87837	0.88242	0.88608	0.89243	0.88956	0.91204	0.91567
burn time (sec)	91	92	92	91	91.5	90	89
Second Stage							
?V (ft/sec)	22653	22653	22653	22653	22653	22653	22653
$[\cos(?)]_{ave}$	0.18120	0.17560	0.17373	0.16605	0.16690	0.16334	0.15641
burn time (sec)	248	244	240	238.5	237.5	234	231
Wpay (lbf)	36259	31491	26646	22146	17197	16166	8432
POST Output							
Wpay (lbf)	30974	26355	21928	17559	12058	10026	5439
Difference between payload weights	5284	5136	4718	4586	5139	6140	2992

4.1.1.7 Rkt-Rkt Performance Analysis

The mass fraction analysis was conducted using an ideal Rkt-Rkt trajectory, as described in section 3, based on the previous sensitivity analyses. The ideal Rkt-Rkt RLV trajectory baseline configuration is detailed in Table 14. The inert mass fractions of both stages were varied from 0.08 to 0.25. The payload weights determined by POST decreased with increasing inert mass fractions as shown in Table 15. Inert mass fraction values greater than 0.19 resulted in insufficient fuel for the vehicle to reach orbit given the fixed GTOW. As shown in Table 15, the payload weight increases by almost 40,000 lbf as the inert mass fractions decreases over the range shown. This extreme sensitivity of payload weight to inert mass fraction shows the importance of low inert mass fractions for the Rkt-Rkt RLV. POST's payload weight data was verified by the rocket analysis, which revealed a close correlation

between the rocket analysis payload weights and those computed via POST, as shown in Table 15.

Table 14: Ideal Rkt-Rkt Trajectory Baseline Configuration

APTSS RLV ID	**Rkt-Rkt**
Staging Dynamic Pressure (lbf/ft^2)	350
Staging Mach Number	7
Max Dynamic Pressure (lbf/ft^2)	475
Drag coefficient	.25
Axial G-load Limit	6

Table 15: Trajectory and Mass Data from the Rkt-Rkt Mass Fraction Analyses

Both Stages Inert Mass Fraction	**0.08**	**0.1**	**0.12**	**0.14**	**0.16**	**0.18**	**0.19**
Rocket Equation Output							
First stage							
? V (ft/sec)	5982	5992	5981	5983	5992	6272	6229
$[\cos(?)]_{ave}$	0.67627	0.66459	0.66508	0.67205	0.67985	0.71286	0.74789
burn time (sec)	125	130	127	127	128	132	131
Second Stage							
?V (ft/sec)	18602	18592	18603	18601	18592	18312	18335
$[\cos(?)]_{ave}$	0.20452	0.13696	0.17627	0.17320	0.17539	0.15334	0.15641
burn time (sec)	160	157	155	154	152	148	149
Wpay (lbf)	48933	41319	30789	21885	13411	7537	3763
POST Output							
Wpay (lbf)	44033	36617	28892	20632	13267	7510	3141
Difference between payload weights	4899	4701	1897	1253	143	27	621

4.1.2 Rkt-RBCC Configuration

The analysis of the Rkt-RBCC vehicle found that the RLV had insufficient fuel to reach orbit using any of the 2nd stage inert mass fractions shown in Table 4. The 2nd stage RBCC yielded a heavy 2nd stage inert weight, but produced minimal thrust when compared with a pure rocket only. The scramjet component of the engine produced one tenth of the total thrust when first activated. The scramjet burned for only 56 seconds. Just prior to the engine shutdown the engine produced a measly one-one thousandth of the total vehicle thrust. This drastic decrease in thrust resulted from the vehicle's high altitude. At the baseline inert mass fraction of 0.30 the vehicle required an extra 92,947 pounds of fuel to reach orbit, with no payload capability. Using the lowest 2nd stage inert mass fraction for a RBCC as shown in Table 4, a value of 0.23, the RLV required 45,470 pounds of extra fuel to reach orbit. Additional analyses revealed that 2nd stage inert mass fractions less than 0.15 permitted the RLV to reach orbit without needing additional fuel, but the RLV was eliminated from further consideration since this inert mass fraction was so far outside the published range for RBCC engines. These results show that given the predicted mass fractions for the vehicle, the Rkt-RBCC configuration is not feasible.

4.1.3 TJ-Rkt1 Configuration

4.1.3.1 TJ-Rkt1 Sensitivity Analysis

Sensitivity analysis was attempted for the TJ-Rkt1 RLV, but efforts proved fruitless. POST failed to converge upon a solution when any change was made to the TJ-Rkt1 trajectory input file. This problem was the same seen during the sensitivity analysis of the Rkt-Rkt vehicle,

but the problem was so severe that it prevented completion of any sensitivity analysis. Additional trajectories were not created, in order to conduct the analysis, due to the time intensive nature of creating or amending trajectories. The TJ-Rkt1 vehicle's performance was subsequently based on the trajectory assumptions detailed in Table 5.

4.1.3.2 TJ-Rkt1 Performance Analysis

The inert mass fraction analyses revealed that varying the 1st stage mass fraction over the range found in the literature review had little effect on payload weight. This is shown in Table 16, where the payload weight increased by only 452 lbf as the 1st stage inert mass fraction was decreased from 0.44 down to 0.29. Conversely, over this same range, the inert weight decreased by almost 5,000 lbf. These results show that 1st stage inert weight reductions do not greatly improve payload weight, but they do reduce total inert weight.

These results are reasonable using the methodology conceived for this study. By reducing the 1st stage inert mass fraction, the 2nd stage total weight was increased by the amount of weight saved from the 1st stage inert weight reduction. This extra 2nd stage total weight was lifted into orbit by the low efficiency rocket engines, which burned excessive amounts of fuel to lift the additional weight. Additionally, the extra 2nd stage total weight resulted in small increases in the 2nd stage inert weight. Although the trajectories with the lower 1st stage inert mass fractions had a larger W_{orbit}, the majority of the additional W_{orbit} was consumed by the extra 2nd stage propellant and inert weights. This resulted in only slight payload increases as the 1st stage inert mass fraction decreased.

Table 16: Weight Data for 1st Stage Inert Mass Fraction Analysis of TJ-Rkt1 RLV

F_2	0.1	0.1	0.1	0.1	0.1	0.1	0.1	0.1
F_1	0.44	0.41	0.39	0.37	0.35	0.33	0.31	0.29
GTOW (lbf)	1000000	1000000	1000000	1000000	1000000	1000000	1000000	1000000
W_{stg} **(lbf)**	860011	860026	859984	859984	859984	859983	859982	859984
W_{prop1} **(lbf)**	139989	139974	140016	140016	140016	140017	140018	140016
W_{tot1} **(lbf)**	249980	237244	229534	222247	215409	208980	202924	197205
W_{inert1} **(lbf)**	109991	97270	89518	82231	75393	68963	62906	57189
$W_{initial2}$ **(lbf)**	750019	762755	770465	777752	784590	791019	797075	802794
W_{tot2} **(lbf)**	725058	737663	745271	752529	759325	765518	771697	777380
W_{inert2} **(lbf)**	72505	73766	74527	75252	75932	76551	77169	77738
W_{orbit} **(lbf)**	97467	98859	99721	100476	101198	102053	102548	103152
W_{prop2} **(lbf)**	652552	663896	670744	677276	683392	688966	694527	699642
W_{pay} **(lbf)**	24961	25092	25193	25223	25265	25501	25378	25413
Total Inert Weight (lbf)	182497	171036	164045	157484	151325	145515	140076	134927

The inert mass fraction analyses revealed that varying the 2nd stage mass fraction over the range found in the literature review had a large effect on payload weight. This is shown in Table 16, where the payload weight decreased 33,764 lbf as the 2nd stage inert mass fraction was increased from 0.08 up to 0.12. Over this same range there was a 33,765 lbf increase in the vehicle's inert weight. This data clearly shows that reducing the 2nd stage inert weight by 1 lbf directly yields 1 lbf of additional payload weight. The data also revealed that the RLV had

insufficient fuel to reach orbit, given the fixed GTOW, when the 2nd stage inert mass fraction was greater than 0.13.

Table 17: Weight Data for 2nd Stage Inert Mass Fraction Analysis of TJ-Rkt1 RLV

F_2	0.08	0.09	0.1	0.11	0.12
F_1	0.35	0.35	0.35	0.35	0.35
GTOW (lbf)	1000000	1000000	1000000	1000000	1000000
W_{stg} **(lbf)**	859984	859984	859984	859984	859984
W_{prop1} **(lbf)**	140016	140016	140016	140016	140016
W_{tot1} **(lbf)**	215409	215409	215409	215409	215409
W_{inert1} **(lbf)**	75393	75393	75393	75393	75393
$W_{initial2}$ **(lbf)**	784590	784590	784590	784590	784590
W_{tot2} **(lbf)**	742818	742818	742818	742818	742818
W_{inert2} **(lbf)**	59425	59425	59425	59425	59425
W_{orbit} **(lbf)**	101198	101198	101198	101198	101198
W_{prop2} **(lbf)**	683392	683392	683392	683392	683392
W_{pay} **(lbf)**	41772	33609	25265	16733	8008
Total Inert Weight (lbf)	134818	142981	151325	159857	168583

4.1.3.3 Validation of TJ-Rkt1 RLV Results

The thrust data provided in the POST output file was verified at several points along the RLV's 1st stage flight path. The thrust data in the POST output file was divided by the number of engines on the TJ-Rkt1 RLV and verified against the thrust data for one turbojet engine provided by AFRL. The turbojet thrust data, based on flight Mach number and altitude, is shown in Appendix B. Since the turbojet thrust data in Appendix B was given based on even numbers of flight Mach number and altitude, a simple linear interpolation of these values was conducted to verify POST's thrust output. As shown in Table 18, POST's thrust output was

almost exactly the same as the interpolated thrust values from the AFRL engine data for a given flight condition. This verified the accuracy of POST's output.

Table 18: Thrust Data Comparison Between POST's Output File and AFRL Turbojet Data at Various Flight Conditions for TJ-Rkt1 RLV

Flight Condition		Thrust per engine (lbf)	
Mach Number	**Altitude (ft)**	**POST**	**Interpolated AFRL Data**
0	0	51620	51620
1.1	9998	42556	42703
1.5	15179	49321	50086
4	54303	51787	51552

4.1.4 TJ-Rkt2 Configuration

4.1.4.1 TJ-Rkt2 Sensitivity Analysis

Sensitivity analysis was attempted for the TJ-Rkt2 RLV, but efforts proved fruitless. POST failed to converge upon a solution when any change was made to the TJ-Rkt2 trajectory input file. This problem was the same seen during the sensitivity analysis of the TJ-Rkt1 vehicle. Additional trajectories were not created, in order to conduct the analysis, due to the time intensive nature of creating or amending trajectories. The TJ-Rkt2 vehicle's performance was subsequently based on the trajectory assumptions detailed previously in Table 5.

4.1.4.2 TJ-Rkt2 Performance Analysis

The TJ-Rkt2 mass fraction analysis revealed that 1st stage inert mass fraction variations had an unexpected effect on the RLV's payload capacity. As shown in Table 19, the payload weight increased with decreasing 1st stage inert mass fraction. Over the range of 1st stage inert mass fractions shown in Table 19, the payload weight increased by 1138 lbf. This was approximately an 15% increase over the lowest payload weight of 7,748 lbf. .

These results are similar in nature to those found for the TJ-Rkt1 1st stage mass fraction analysis. By reducing the 1st stage inert mass fraction, the 2nd stage total weight was increased by the amount of weight saved from the 1st stage inert weight reduction. This extra 2nd stage total weight was lifted into orbit by the low efficiency rocket engines, which burned excessive amounts of fuel to lift the additional weight. Additionally, the extra 2nd stage total weight resulted in small increases in the 2nd stage inert weight. Although the trajectories with the lower 1st stage inert mass fractions had a larger W_{orbit}, the additional W_{orbit} was consumed by the extra 2nd stage propellant and inert weights. This resulted in decreasing payload weights as the 1st stage mass fraction decreased.

As shown in Table 19, the total inert weight of the vehicle decreased with decreasing 1st stage inert mass fraction. This trend was expected. Over the range of 1st stage inert mass fractions shown in Table 19, the RLV's total inert weight decreased by approximately 4,000lbf.

Table 19: Weight Data for 1st Stage Inert Mass Fraction Analysis of TJ-Rkt2 RLV

$\mathbf{F_2}$	0.1	0.1	0.1	0.1	0.1	0.1	0.1	0.1
$\mathbf{F_1}$	0.44	0.41	0.39	0.37	0.35	0.33	0.31	0.29

GTOW (lbf)	1000000	1000000	1000000	1000000	1000000	1000000	1000000	1000000
W_{stg} (lbf)	881039	880941	881002	880972	881011	880988	881011	881021
W_{prop1} (lbf)	118961	119059	118998	119028	118989	119012	118989	118979
W_{tot1} (lbf)	212430	201794	195078	188933	183060	177629	172447	167576
W_{inert1} (lbf)	93469	82735	76080	69905	64071	58617	53458	48597
$W_{initial2}$ (lbf)	787569	798205	804921	811066	816940	822370	827552	832423
W_{tot2} (lbf)	778958.5	789319	796564.8	802795.2	808836.7	814333.5	819606.9	824675.5
W_{inert2} (lbf)	77895	78931	79656	80279	80883	81433	81960	82467
W_{orbit} (lbf)	86507	87818	88013	88551	88987	89470	89906	90216
W_{prop2} (lbf)	701062	710387	716908	722515	727953	732900	737646	742207
W_{pay} (lbf)	8611	8886	8356	8271	8103	8036	7945	7748
Total Inert Weight (lbf)	171365	161667	155737	150184	144954	140051	135419	131064

The inert mass fraction analyses revealed that varying the 2nd stage mass fraction over the range found in the literature review had a large effect on payload weight. This is shown in Table 20, where the payload weight decreased 17,583 lbf as the 2nd stage inert mass fraction was increased from 0.08 up to 0.1. Over this same range there was a 17,583 lbf increase in the vehicle's inert weight. This data clearly show that reducing the 2nd stage inert weight by 1 lbf directly yields 1 lbf of additional payload weight. The data also revealed that the RLV had insufficient fuel to reach orbit, given the fixed GTOW, when the 2nd stage inert mass fraction was greater than 0.1.

Table 20: Weight Data for 2nd Stage Inert Mass Fraction Analysis of TJ-Rkt2 RLV

F_2	0.08	0.09	0.1
F_1	0.35	0.35	0.35
GTOW (lbf)	1000000	1000000	1000000
W_{stg} (lbf)	881011	881011	881011
W_{prop1} (lbf)	118989	118989	118989
W_{tot1} (lbf)	183060	183060	183060
W_{inert1} (lbf)	64071	64071	64071
$W_{initial2}$ (lbf)	816940	816940	816940
W_{tot2} (lbf)	791253	799948	808836
W_{inert2} (lbf)	63300	71995	80883
W_{orbit} (lbf)	88987	88987	88987
W_{prop2} (lbf)	727953	727953	727953
W_{pay} (lbf)	25686	16991	8103
Total Inert Weight (lbf)	127371	136066	144954

4.1.4.3 Validation of TJ-Rkt2 RLV Results

The thrust data provided in the POST output file was verified at several points along the RLV's 1st stage flight path. The thrust data in the POST output file was divided by the number of engines on the TJ-Rkt2 RLV and verified against the thrust data for one turbojet engine provided by AFRL. The turbojet thrust data, based on flight Mach number and altitude, is shown in Appendix B. Since the turbojet thrust data in Appendix B was given based on even numbers of flight Mach number and altitude, a simple linear interpolation of these values was conducted to verify POST's thrust output. As shown in Table 21, POST's thrust output was almost exactly the same as the interpolated thrust values from the AFRL engine data. This verified the accuracy of POST's output.

Table 21: Thrust Data Comparison Between POST's Output File and AFRL Turbojet Data at Various Flight Conditions for TJ-Rkt2 RLV

Flight Condition		Thrust per engine (lbf)	
Mach Number	**Altitude (ft)**	**POST**	**Interpolated AFRL Data**
0	0	51620	51620
1.02	19587	22775	27201
1.77	29983	39694	40705
4.0	54023	52499	54016

4.1.5 RBCC-Rkt Configuration

The analysis of the RBCC-Rkt vehicle found that the RLV had insufficient fuel to reach orbit using any of the 1st stage inert mass fractions shown in Table 4. The 1st stage RBCC yielded a heavy 1st stage inert weight, but produced minimal thrust when compared with a pure rocket only. The scramjet component of the engine produced one tenth of the total thrust when first activated. At the Mach 4 activation point of the scramjet, the RLV weighed 485,839 pounds while the scramjet provided 42,806 pounds of thrust. This minimal amount scramjet thrust resulted from the vehicle's high altitude. Ultimately this vehicle's large 1st stage inert weight prevented the vehicle from reaching orbit. This problem was similar to that encountered with the Rkt-RBCC RLV. These results show that given the predicted mass fractions for the vehicle, the Rkt-RBCC configuration is not feasible and thus this RLV was eliminated from further consideration.

4.2 RLV Performance Comparison

The results clearly show that the TJ-Rkt1 RLV out-performs the TJ-Rkt2 RLV using both figures of merit. As shown in Table 22, for relatively similar total inert weights, the TJ-Rkt1 RLV payload weights were three times greater than those of the TJ-Rkt2 RLV.

Table 22: Payload and Inert Weights for TJ-Rkt1 and TJ-Rkt2 RLVs

TJ-Rkt1								
Wpay (lbf)	24961	25092	25193	25223	25265	25501	25378	25413
Total Inert Weight (lbf)	182497	171036	164045	157484	151325	145515	140076	134927
TJ-Rkt2								
W_{pay} (lbf)	8611	8886	8356	8271	8103	8036	7945	7748
Total Inert Weight (lbf)	171365	161667	155737	150184	144954	140051	135419	131064
F2	0.1	0.1	0.1	0.1	0.1	0.1	0.1	0.1
F1	0.44	0.41	0.39	0.37	0.35	0.33	0.31	0.29

Comparing the baseline RLV configurations, the Rkt-Rkt RLV had the lowest inert weight and highest payload weight. The TJ-Rkt2 vehicle had the highest inert weight and lowest payload weight. This comparison is shown in Table 23. This comparison is useful because of the uniformity of all rocket and turbojet stage inert mass fractions.

Table 23: Payload and Inert Weights of RLV Configurations

APTSS RLV ID	Rkt-Rkt	TJ-Rkt1	TJ-Rkt2
F_1	0.1	0.35	0.35
F_2	0.1	0.1	0.1

W_{pay} (lbf)	36617	25265	8103
Total Inert Weight (lbf)	100000	140076	144945

Furthermore it was shown that small increases in the 2nd stage inert mass fractions of the TJ-Rkt1 and TJ-Rkt2 vehicles, above the baseline of 0.1, resulted in insufficient fuel for those vehicles to reach orbit. The TJ-Rkt1 vehicle failed to reach orbit when the 2nd stage inert mass fraction was greater than 0.12. The TJ-Rkt2 vehicle failed to reach orbit when the 2nd stage inert mass fraction was greater than 0.1. Comparatively, the Rkt-Rkt RLV had sufficient fuel to reach orbit with inert mass fractions up to 0.19. This showed that the RLVs with airbreathing first stage engines were less tolerant to 2nd stage inert mass variations. Furthermore, it revealed that the rocket 2nd stage drove the performance of the TJ-Rkt1 and TJ-Rkt2 RLVs.

4.3 Usefulness of Methodology

The methodology for determining RLV performance using the prescribed methodology worked well. As shown in the previous results, the method produced accurate payload and inert weights for a wide range of RLVs.

The primary problem with using POST was the steep learning curve. The archaic Fortran 77 input code format led to many frustrating days of research. After a solid month of using POST, the numerous syntax errors were isolated and understood. In addition to syntax problems, building the actual vehicle trajectories that converged to the final orbit was time consuming. Each trajectory took near a month to create. The majority of these problems centered on the assumptions for the RLVs. Many of the early trajectories failed to make orbit

or even achieve staging conditions, instead crashing into the Earth. Some vehicles would accelerate too quickly and shoot past the orbital altitude. Given the large number of variables involved and often useless POST output it was difficult to isolate the problems in each trajectory in order to prescribe a fix. These problems were exacerbated by the fact that most of the data for the vehicles was assumed, instead of having a well characterized vehicle.

Another major problem with POST was the sensitivity of the trajectory to any changes. This had a detrimental effect on the sensitivity analysis of the TJ-Rkt1 and TJ-Rkt2 vehicles. Minor changes to quantities such as maximum g-limit, dynamic pressures, and engine ISP caused the TJ-Rkt1 and TJ-Rkt2 trajectories to fail. The Rkt-Rkt trajectory converged when there were small variations in the trajectory constraints, but major changes to input variables during the sensitivity analysis caused the vehicle to crash or shoot out of orbit. This problem limited the scope of the sensitivity analysis because there was insufficient time to generate a new vehicle trajectory each time the trajectory failed to converge. This problem was most prevalent in the TJ-Rkt1 and TJ-Rkt2 trajectories, but this phenomenon cannot be explained.

One of the more bizarre, but rare, problems with POST happened during the Rkt-Rkt staging Mach number sensitivity analysis. Trajectories with staging Mach numbers greater than Mach 7 gained altitude too quickly without achieving the required orbital speed. This phenomenon is depicted in Figure 18. The vehicles over-shot the desired altitude and returned to the correct altitude via pitching maneuvers while the vehicle gained the required velocity. The POST output file indicated that the program converged on a solution, which indicated that the

trajectory was optimized. Based on the unorthodox flight path, these results were discarded. The inflexibility of the trajectories was suspected for this anomaly.

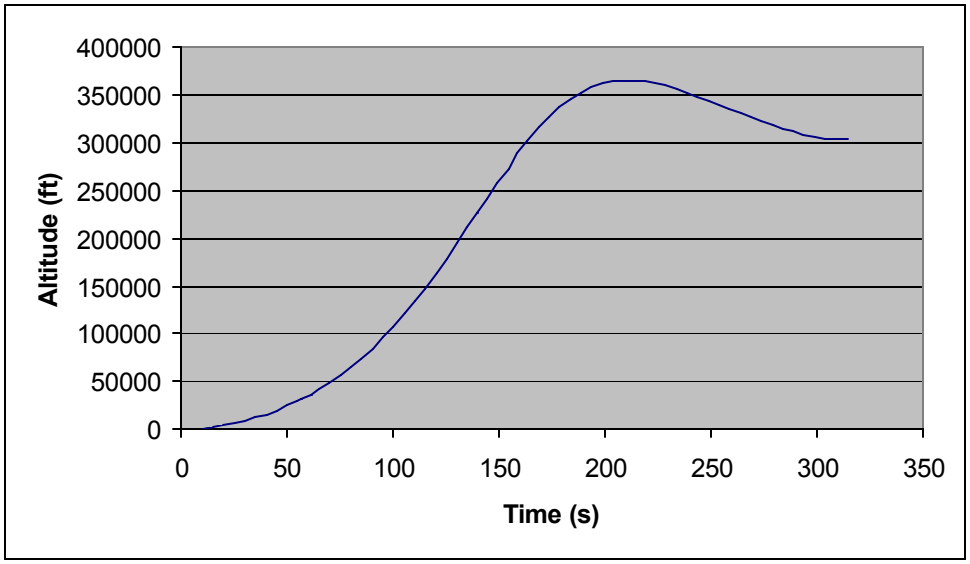

Figure 18: Rkt-Rkt Staging Mach Number of 7.5 Trajectory Time vs. Altitude

5. Conclusions and Recommendations

5.1 RLV Performance

1. Payload and inert weights of all vehicles were most sensitive to variations in the rocket stage inert mass fractions. The TJ-Rkt1 and TJ-Rkt2 vehicles were particularly sensitive because their high first stage weights made 2nd stage weight reductions very important to performance. The TJ-Rkt1 vehicles could not lift payloads into orbit when the rocket inert mass fraction was greater than 0.12, while the TJ-Rkt2 needed an inert mass fraction less than or equal to 0.10. In contrast, the Rkt-Rkt vehicle could place a small payload into orbit at inert mass fractions as high as 0.19. The TJ-Rkt1 and TJ-Rkt2 vehicle performance was relatively insensitive to 1st stage mass fractions. This indicated that technological advances in rocket technology are most important to improving performance of all the vehicles studied.

2. Based on the aerodynamic data and engine data used, horizontal takeoff was far superior to vertical takeoff for RLVs with turbojet powered 1st stages. The TJ-Rkt1 RLV payload capability was almost three times as great as that of the TJ-Rkt2 vehicle. Using more accurate aerodynamic data may indicate that the horizontal takeoff vehicle's performance gains are even greater because the vehicle may not require so many turbojet engines to overcome drag at low Mach numbers, while any vertical takeoff vehicle will still require a large number of engines to provide the high T/W ratio needed for launch. This reduction in turbojet engines for may reduce fuel consumption and increase payload weight for a horizontally launched RLV.

3. The extreme number of engines need by the vertical takeoff turbojet first stage RLV indicate that this configuration is completely impractical for operational use. If future advances in turbine technology yield a high-thrust, low-weight turbine engine then the RLV may become feasible, but it will still not outperform the horizontal takeoff RLV. Advancements in turbine technology of this kind could reduce first stage inert weight and the number of turbine engines needed for the vertical takeoff RLV, but based on the results of this study it would be more advantageous to use these new high-performance turbine engines on the horizontal takeoff turbojet first stage RLV.

4. Based on this engine and aerodynamic data, RBCC engines should not be used for direct ascent trajectories. They both provide too little thrust during scramjet mode and operate for too short of a Mach range and time period to overcome their prohibitive weight. It can be surmised that RBCC powered vehicles in a direct ascent trajectory will ultimately fail unless RBCC engine weights decrease substantially.
Different aerodynamic and engine data may indicate that direct ascent is feasible with an RBCC engine, but this is unlikely,

5. Of all five types of RLVs studied, a TSTO with two rocket stages has the most potential for future use. All vehicles were configured with a rocket stage mass fraction of 0.1. This is an optimistic value when compared to the range found in the literature of 0.08-0.25. If technology advances fail to reduce the rocket inert mass fraction to levels near the low end of that range, it is unlikely that a RLV similar to the TJ-Rkt1 or TJ-Rkt2 vehicles would be viable. Given that the Rkt-Rkt vehicle could lift payloads into orbit at high rocket stage inert mass

fractions, the development of a TSTO with two rocket stages is less dependant on these technological advances.

5.2 Methodology

1. The methodology devised in this research is an effective and accurate means for AFRL to utilize when comparing RLVs. This method will allow AFRL to accurately compare different RLV proposals from contractors to determine if the contractor's performance estimates are realistic. AFRL can further use this method to determine which potential RLVs concepts require further study and which ones should be discarded.

2. This methodology may not be ideal for performing a sensitivity analysis of various trajectory constraints for all types of RLVs. The problems encountered with the sensitivity analysis may be due to limitations of optimization program. A more simple analysis program may be required for sensitivity analysis, or more time may be needed to research this problem.

3. Ultimately, the benefits of this method outweigh the steep learning curve to using POST, the time consuming process of altering trajectories, and the difficulties encountered with the sensitivity analysis.

5.3 Recommendations

1. More accurate engine and aerodynamic data must be obtained. Air-augmented rocket data should be used in conjunction with the scramjet data to model RBCC performance. Ramjet data should be combined with turbojet and scramjet data to model a TBCC engine. Better low speed aerodynamic data, in the Mach 1-5 range, must be obtained to reduce the large drag on the TJ-Rkt RLVs.

2. Further study on the TJ-Rkt1 and TJ-Rkt2 vehicles should continue to determine if a sensitivity analysis of these vehicles is possible using POST.

3. A performance study should be accomplished using RBCC and TBCC first stages in a lifting ascent trajectory. A RBCC second stage vehicle in a lifting trajectory should also be studied.

Appendix A: X-43 Aerodynamic Properties

Mach Number	Angle of Attack (a)	Lift Coefficient	Drag Coefficient
0.3	-10	-0.7884	0.158016
	-5	-0.4012	0.078816
	0	0.0126	0.069
	5	0.4548	0.092352
	10	0.7839	0.160224
	15	0.9761	0.277536
	20	1.0686	0.38016
0.6	-10	-0.7884	0.158016
	-5	-0.4012	0.078816
	0	0.0126	0.069
	5	0.4548	0.092352
	10	0.7839	0.160224
	15	0.9761	0.277536
	20	1.0686	0.38016
0.9	-10	-0.7884	0.19752
	-5	-0.4012	0.09852
	0	0.0126	0.08625
	5	0.4548	0.11544
	10	0.7839	0.20028
	15	0.9761	0.34692
	20	1.0686	0.4752
1	-10	-0.7884	0.2469
	-5	-0.4012	0.12315
	0	0.0126	0.08625
	5	0.4548	0.1443
	10	0.7839	0.25035
	15	0.9761	0.43365
	20	1.0686	0.594
1.5	-10	-0.7884	0.202
	-5	-0.4012	0.1095
	0	0.0126	0.0782
	5	0.4548	0.1171
	10	0.7839	0.2009
	15	0.9761	0.3114
	20	1.0686	0.4294

Mach Number	Angle of Attack (a)	Lift Coefficient	Drag Coefficient
2	-10	-0.5918	0.1646
	-5	-0.2864	0.0821
	0	0.0259	0.0575
	5	0.3437	0.0962
	10	0.6044	0.1669
	15	0.8541	0.2891
	20	0.9601	0.396
3	-10	-0.3909	0.1123
	-5	-0.1852	0.0549
	0	0.0179	0.0389
	5	0.2209	0.0632
	10	0.4273	0.1293
	15	0.6409	0.2421
	20	0.7918	0.3544
4	-10	-0.3126	0.0924
	-5	-0.1459	0.045
	0	0.0156	0.0322
	5	0.1769	0.0525
	10	0.3438	0.1074
	15	0.5193	0.2009
	20	0.7054	0.3398
5	-10	-0.2713	0.0817
	-5	-0.1247	0.0394
	0	0.0145	0.0282
	5	0.1535	0.0465
	10	0.3003	0.096
	15	0.459	0.1811
	20	0.6297	0.3076
6	-10	-0.2462	0.0755
	-5	-0.1115	0.0361
	0	0.0139	0.0259
	5	0.1391	0.0431
	10	0.274	0.0895
	15	0.4234	0.1699
	20	0.587	0.2903
8	-10	-0.2179	0.0691
	-5	-0.0962	0.0327
	0	0.0133	0.0236
	5	0.1225	0.0395
	10	0.2444	0.0827
	15	0.3846	0.1585
	20	0.542	0.2732

Mach Number	Angle of Attack (a)	Lift Coefficient	Drag Coefficient
10	-10	-0.203	0.066
	-5	-0.0879	0.0309
	0	0.0131	0.0223
	5	0.1136	0.0377
	10	0.2288	0.0794
	15	0.3649	0.1532
	20	0.52	0.2656
12	-10	-0.1933	0.0706
	-5	-0.0823	0.0365
	0	0.0129	0.0283
	5	0.1075	0.0432
	10	0.2185	0.0836
	15	0.3523	0.1554
	20	0.5064	0.2651
15	-10	-0.1848	0.0742
	-5	-0.0774	0.0405
	0	0.0127	0.0325
	5	0.102	0.0473
	10	0.2095	0.087
	15	0.3414	0.1577
	20	0.4947	0.2653
25	-10	-0.1753	0.0726
	-5	-0.0714	0.0401
	0	0.0128	0.0326
	5	0.0954	0.0468
	10	0.1997	0.0839
	15	0.3304	0.1534
	20	0.4828	0.2617

Appendix B: Engine Data

AFRL Mach 4.4 Turbojet Thrust (lbf)

Mach Number	0	0.5	0.8	1	1.5	2	2.5	3	3.25	3.75	4
Altitude (ft)											
0	51621	54326	51785	53721	74073	0	0	0	0	0	0
5000	0	47598	39940	45774	65959	0	0	0	0	0	0
10000	0	0	33160	38853	58108	81412	127578	0	0	0	0
20000	0	0	22508	26583	42066	65315	100391	146736	0	0	0
30000	0	0	14923	17615	29340	48284	71157	100641	0	0	0
40000	0	0	9584.4	11293	19106	31506	46397	65463	74388	92791	103912
42000	0	0	0	10254	17324	28618	42120	59417	67514	84201	94279
50000	0	0	0	6966.7	11778	19448	28620	40321	45834	57072	63871
60000	0	0	0	4295	7270.1	11984	17650	24826	28208	35084	39236
70000	0	0	0	2638.8	4479.5	7362.4	10815	15206	17256	21419	23971
72000	0	0	0	2391.9	4063.7	6669.8	9792.5	13770	15619	19403	21696
80000	0	0	0	1620.7	2748.4	4502.2	6610.1	9293.5	10525	13053	14604
90000	0	0	0	1005	1700.8	2780.2	4071.7	5719.5	6468	8007.4	8954.3
100000	0	0	0	627.4	1058.2	1727.3	2526.8	3548	4003	4945.4	5535.9

AFRL Mach 4.4 Turbojet Isp (sec)

Mach Number	0	0.5	0.8	1	1.5	2	2.5	3	3.25	3.75	4
Altitude (ft)											
0	2122.1	1957.1	1765.5	1719.4	1605.4	0	0	0	0	0	0
5000	0	1963.6	1776.4	1731.2	1640.8	0	0	0	0	0	0
10000	0	0	1759.1	1745.2	1674.3	1558.7	1563	0	0	0	0
20000	0	0	1732.6	1731	1719.8	1671.2	1652.7	1605.6	0	0	0
30000	0	0	1717.3	1716.2	1765.1	1751.7	1708.5	1649	0	0	0
40000	0	0	1721.4	1718.3	1786.9	1780.2	1734.7	1676.4	1630	1534.9	1501.1

42000	0	0	0	1717.6	1783.6	1779.4	1733.7	1675.1	1628	1533.4	1499.4
50000	0	0	0	1714.2	1780.9	1776.4	1729.8	1669.8	1623	1526.7	1492.1
60000	0	0	0	1708.9	1777.6	1769.5	1724.5	1662.6	1615	1517.6	1482.3
70000	0	0	0	1702.6	1775	1763.2	1714	1650.8	1602	1502.7	1467.6
72000	0	0	0	1701	1773.8	1760.2	1710.8	1647.3	1598	1498.9	1463.7
80000	0	0	0	1694.4	1764.8	1747.3	1698	1633.3	1582	1481.5	1446.8
90000	0	0	0	1688.3	1756.2	1734.4	1681.9	1615.5	1563	1459.6	1424.3
100000	0	0	0	1681.8	1745.7	1720.3	1666.4	1598.1	1543	1437.9	1402.5

HRE Derived Scramjet Data

Mach Number	Altitude (ft)	Thrust Coefficient	Isp (sec)
4	56000.	0.570	1294
	72000.	0.564	1286
	85800.	0.610	1272
4.5	61500.	0.693	1139
	76500.	0.799	1133
	91000.	0.779	1115
5	66000.	0.809	996
	80500.	1.017	981
	91500.	1.075	941
5.5	70000.	1.034	870
	84600.	1.099	838
	99700.	1.063	813
6	73500.	1.022	746
	88300.	1.078	723
	103500.	1.037	698
6.5	77000.	1.006	639
	92000.	1.037	615
	107000.	0.983	588
7	80000.	0.977	538
	95050.	0.955	512
	110000.	0.886	479
7.5	83000.	0.895	438.8
	98100.	0.848	411
	133500.	0.755	369
8	85800.	0.784	342
	101000.	0.705	312
	116500.	0.585	261
8.5	88400.	0.613	245.7
	104000.	0.553	213
	11950.	0.375	153

Appendix C: Rkt-Rkt Weight Data

Rkt-Rkt 1 Aerodynamic Analysis Weight Breakdown					
X-43 Drag Coefficient Multiplier	0.0 Cd	0.25 Cd	0.5 Cd	0.75 Cd	1.0 Cd
GTOW (lbf)	1000000	1000000	1000000	1000000	1000000
W_{stg} (lbf)	605388	576000	573396	557105	540366
W_{prop1} (lbf)	394612	424000	426604	442895	459634
W_{tot1} (lbf)	438458	471111	474004	492106	510704
W_{inert1} (lbf)	43846	47111	47400	49211	51070
$W_{initial2}$ (lbf)	561542	528889	525996	507894	489296
W_{tot2} (lbf)	542504	509877	507185	489733	471727
W_{inert2} (lbf)	54250	50988	50719	48973	47173
W_{orbit} (lbf)	73289	70000	69529	67135	64741
W_{prop2} (lbf)	488253	458889	456467	440759	424555
W_{pay} (lbf)	19039	19012	18810	18162	17568

Maximum g-limit Analysis Weight Breakdown							
Maximum g-limit	3.0g	3.5g	4g	4.5g	5g	5.5g	6g
GTOW (lbf)	1000000	1000000	1000000	1000000	1000000	1000000	1000000
W_{stg} (lbf)	540831	540825	540938	540992	541039	541062	541074
W_{prop1} (lbf)	459169	459175	459062	459008	458961	458938	458926
W_{tot1} (lbf)	510188	510194	510069	510009	509957	509931	509918
W_{inert1} (lbf)	51019	51019	51007	51001	50996	50993	50992
$W_{initial2}$ (lbf)	489812	489806	489931	489991	490043	490069	490082
W_{tot2} (lbf)	472406	472247	472329	472465	472587	472670	472727
W_{inert2} (lbf)	47241	47225	47233	47246	47259	47267	47273
W_{orbit} (lbf)	64647	64783	64835	64773	64715	64666	64628
W_{prop2} (lbf)	425165	425023	425096	425218	425328	425403	425454
W_{pay} (lbf)	17406	17558	17602	17527	17456	17399	17355

Rocket Isp Analysis Weight Breakdown							
Isp (sec)	400	390	380	370	360	350	340
GTOW (lbf)	1000000	1000000	1000000	1000000	1000000	1000000	1000000
W_{stg} (lbf)	566784	558523	549875	540876	531602	521852	511779
W_{prop1} (lbf)	433216	441477	450125	459124	468398	478148	488221
W_{tot1} (lbf)	481351	490530	500139	510138	520442	531276	542468
W_{inert1} (lbf)	48135	49053	50014	51014	52044	53128	54247
$W_{initial2}$ (lbf)	518649	509470	499861	489862	479558	468724	457532
W_{tot2} (lbf)	487674	483114	477932	472302	467500	458698	452092
W_{inert2} (lbf)	48767	48311	47793	47230	46750	45870	45209
W_{orbit} (lbf)	79742	74667	69722	64790	58808	55896	50649
W_{prop2} (lbf)	438907	434803	430139	425072	420750	412828	406883
W_{pay} (lbf)	30975	26356	21929	17560	12058	10026	5440

Maximum Dynamic Pressure Analysis Weight Breakdown						
Maximum Dynamic Pressure (lbf/ft^2)	Baseline	575	550	525	500	475
GTOW (lbf)	1000000	1000000	1000000	1000000	1000000	1000000
W_{stg} (lbf)	540876	540703	540287	539833	539239	525994
W_{prop1} (lbf)	459124	459297	459713	460167	460761	474006
W_{tot1} (lbf)	510138	510330	510792	511297	511957	526673
W_{inert1} (lbf)	51014	51033	51079	51130	51196	52667
$W_{initial2}$ (lbf)	489862	489670	489208	488703	488043	473327
W_{tot2} (lbf)	472302	472108	471908	471191	470407	456142
W_{inert2} (lbf)	47230	47211	47191	47119	47041	45614
W_{orbit} (lbf)	64790	64773	64491	64631	64677	62799
W_{prop2} (lbf)	425072	424897	424717	424072	423366	410528
W_{pay} (lbf)	17560	17562	17300	17512	17636	17185

Staging Dynamic Pressure Analysis Weight Breakdown							
Staging Dynamic Pressure (lb/ft^2)	350	325	300	280	260	240	2
GTOW (lbf)	1000000	1000000	1000000	1000000	1000000	1000000	10000
W_{stg} (lbf)	540366	540050	539095	538301	537269	536553	5351
W_{prop1} (lbf)	459634	459950	460905	461699	462731	463447	4648
W_{tot1} (lbf)	510704	511056	512117	512999	514146	514941	5164
W_{inert1} (lbf)	51070	51106	51212	51300	51415	51494	516
$W_{initial2}$ (lbf)	489296	488944	487883	487001	485854	485059	4835
W_{tot2} (lbf)	471727	471390	470386	469638	469016	468952	4683
W_{inert2} (lbf)	47173	47139	47039	46964	46902	46895	468
W_{orbit} (lbf)	64741	64693	64536	64327	63740	63002	620
W_{prop2} (lbf)	424555	424251	423347	422674	422114	422057	4215
W_{pay} (lbf)	17568	17554	17497	17363	16838	16107	151

Mach Number Analysis Weight Breakdown					
Mach Number	Mach 3.0	Mach 4.0	Mach 5.0	Mach 6.0	Mach 7.0
GTOW (lbf)	1000000	1000000	1000000	1000000	1000000
W_{stg} (lbf)	540876	486409	438719	396729	350334
W_{prop1} (lbf)	459124	513591	561281	603271	649666
W_{tot1} (lbf)	510138	570657	623646	670301	721851
W_{inert1} (lbf)	51014	57066	62365	67030	72185
$W_{initial2}$ (lbf)	489862	429343	376354	329699	278149
W_{tot2} (lbf)	472302	406488	350117	301508	249722
W_{inert2} (lbf)	47230	40649	35012	30151	24972
W_{orbit} (lbf)	64790	63504	61249	58342	53399
W_{prop2} (lbf)	425072	365839	315105	271357	224750
W_{pay} (lbf)	17560	22855	26237	28191	28427

Rocket Stage Mass Fraction Analysis Weight Breakdown							
Rocket Stage Mass Fraction	0	0	0	0	0	0	0
GTOW (lbf)	1000000	1000000	1000000	1000000	1000000	1000000	1000000
W_{stg} (lbf)	402577	402553	402535	402550	402056	402553	381451
W_{prop1} (lbf)	597423	597447	597465	597450	597944	597447	618549
W_{tot1} (lbf)	649373	663830	678938	694709	711838	728594	763641
W_{inert1} (lbf)	51950	66383	81473	97259	113894	131147	145092
$W_{initial2}$ (lbf)	350627	336170	321063	305291	288162	271406	236359
W_{tot2} (lbf)	306594	299552	292170	284658	274894	263895	233218
W_{inert2} (lbf)	24527	29955	35060	39852	43983	47501	44311
W_{orbit} (lbf)	68561	66573	63953	60485	57251	55012	47453
W_{prop2} (lbf)	282066	269597	257110	244806	230911	216394	188906
W_{pay} (lbf)	44034	36618	28893	20633	13268	7511	3142

References

1. Anderson, John D. Fundamentals of Aerodynamics (2nd Edition). New York: McGraw-Hill Publishing Company, 1991.

2. Andrews, Earl H. "Scramjet Development and Testing in the United States." AIAA-2001-1927, AIAA/NAL-NASDA-ISAS 10th International Space Planes and Hypersonic Systems and Technologies Conference, Kyoto, Apr 2001.

3. Bilardo, V. J. and others. "The Benefits of Hypersonic Airbreathing Launch Systems for Access to Space." 39th AIAA/ASME/SAE/ASEE Joint Propulsion Conference, AIAA-2003-5265, July 2003.

4. Bowcutt, Kevin and others. "Performance, Operational and Economic Drivers of Reusable Launch Vehicles." AIAA-2002-3901, 38th Joint Propulsion Conference, Indianapolis, July 2002.

5. Chase, Ramon and Ming Tang. "The Quest for Single Stage Earth-to-Orbit: TAV, NASP, DC-X and X-33 Accomplishments, Deficiencies, and Why They Did Not Fly." AIAA-2002-5143, 11th AIAA/AAAF International Conference Space Planes and Hypersonic Systems and Technologies, Orleans, September 2002.

6. Crocker, Andrew M. and others. "A Comparison of Horizontal Takeoff RLVs for the Next Generation Space Transportation." AIAA-2003-5037, July 2003.

7. Czysz, Paul A. and Christopher P. Rahaim. "Perspective of Launch Vehicle Size and Weight Based on Propulsion System Concept." IAC-02-V.4.08, 53rd International Astronautical Congress, Houston, October 2002.

8. Department of the Air Force. Mission Need Statement: Operationally Responsive Spacelift. AFSPC 001-01. Colorado Springs: HQ AFSPC/DRS, 20 December 01.

9. Department of the Air Force. Why and Whither Hypersonics Research in the US Air Force. SAB-TR-00-03. December 2000.

10. Dornhiem, Michael A. "Quick, Cheap Launch," *Aviation Week and Space Technology*, 7 April 2003.

11. Escher, Daric W. and Eric R. Christensen. "Propulsion Technology Impacts on Airbreathing/Rocket Powered TSTO Concepts." AIAA-2002-4328, 38th AIAA/SAE/ASME/ASEE Joint Propulsion Conference, Indianapolis, July 2002.

12. Escher, William J.D. "Combined-Cycle and Hypersonic Propulsion – A Renewed Rocketdyne Initiative." The Synerjet Engine: Airbreathing/Rocket Combined-Cycle Propulsion for Tomorrow's Space Transports. Reprinted from Rocketdyne's Threshold magazine. SAE PT-54, 1997.

13. Escher, William J. D. "On the Airbreathing/Rocket Propulsion Relationship: For Advanced Spaceflight Systems it's the Combination that Counts." AIAA-2003-5266, 39th AIAA/ASME/SAE/ASEE Joint Propulsion Conference, Huntsville, July 2003.

14. Escher, William J. D. "Synerjet for Earth/Orbit Propulsion: Revisiting the 1966 NASA/Mardquart Composite (Airbreathing/Rocket) Propulsion System Study." The Synerjet Engine: Airbreathing/Rocket Combined-Cycle Propulsion for Tomorrow's Space Transports. Reprinted from AIAA Paper 96-3040. SAE PT-54, 1997.

15. Grallert, H. "Synthesis of a FESTIP Airbreathing TSTO Space Transportation System." *Journal of Propulsion and Power*, Vol 17, Number 6. December 2001.

16. Gregory, Tom and others. "Two Stage to Orbit Airbreathing and Rocket System for Low Risk, Affordable Access to Space." SAE 941168. SAE 1994 Atlantic Conference and Exposition, Dayton, April 1994.

17. Heiser, William H. and David T. Pratt. Hypersonic Airbreathing Propulsion. AIAA Educational Series. Washington D.C.: American Institute of Aeronautics and Astronautics, 1994.

18. Hill, Philip and Carl Peterson. Mechanics and Thermodynamics of Propulsion (2nd Edition). New York: Addison-Wesley Publishing Company, 1992.

19. Humble, Ronald W. and others. Space Propulsion Analysis and Design (Revised). New York: McGraw-Hill Publishing Company, 1995.

20. Isakowski, Steven J. and others. International Reference Guide to Space Launch Systems. 3rd Edition. Reston, 1999.

21. Mehta, Unmeel B. "A Two-Stage-To-Orbit Spaceplane Concept with Growth Potential." AIAA-2001-1795, AIAA/NAL-NASDA-ISAS 10th International Space Planes and Hypersonic Systems and Technologies Conference, Kyoto, Apr 2001.

22. Moses, P. L. and others. "An Airbreathing Launch Vehicle Design with Turbine-Based Low-Speed Propulsion and Dual Mode Scramjet High-Speed Propulsion." AIAA-99-4948, 9th International Space Planes and Hypersonic Systems and Technologies Conference, Norfolk, November 1999.

23. NASA Facts. "Hypersonics: Research and Development," NASA Marshall Spaceflight Center, October 2002.

24. NASA Facts. "NASA 'Hyper-X' Program Demonstrates Scramjet Technologies," NASA Langley Research Center, July 2002.

25. "National Aerospace Initiative Objectives," http://www.dod.mil/ddre/nai/objectives.html. 12 September 2003.

26. Nelson, Karl William. Experimental Investigation of an Ejector Scramjet RBCC at Mach 4.0 and Mach 6.5 Simulated Flight Conditions. Ph.D Dissertation, University of Alabama, Huntsville, 2002.

27. Program to Optimize Simulated Trajectories. NASA Langley Research Center and Martin Martietta Corporation. October 1997.

28. Sarigul-Klijn, Marti and Nesrin Sarigul-Klijn. "A Study of Air Launch Methods for RLVs." AIAA 2001-4619, 2001.

29. Snyder, Lynn E. and Daric W. Escher. "High Mach Turbine Engines for Access to Space Launch Systems." AIAA-2003-5036, 39th AIAA Joint Propulsion Conference, Huntsville, July 2003.

30. www.pratt-whitney.com/prod_space_rd180.asp. January 2004.

31. Hamilton, Capt Christopher. Air Force Research Laboratory, Propulsion Directorate. Personal Interview. June 2003.

Vita

Captain Marc A. Brock graduated from Pine Bush High School in Pine Bush, New York. He entered undergraduate studies at Syracuse University in Syracuse, New York where he graduated with a Bachelor of Science degree in Aerospace Engineering in May 1998. He was commissioned through the Detachment 535 AFROTC at Syracuse University. In December 2002 he was awarded a Master of Engineering Degree in Engineering Mechanics from the University of Florida in Gainesville, Florida.

His first assignment was at Vandenberg AFB as a student in Undergraduate Space and Missile Training February 1999. In June 1999, he was assigned to the 20th Space Surveillance Squadron, Eglin AFB, Florida, where he served as a Space Operations Crew Commander. While stationed at Eglin, he served as the Chief, Operations Training and directed all unit level mission-ready training. In May 2003, he entered the Graduate School of Engineering and Management, Air Force Institute of Technology. Upon graduation, he will be assigned to the Space Warfare Center.

REPORT DOCUMENTATION PAGE

Form Approved
OMB No. 074-0188

SE DO NOT RETURN YOUR FORM TO THE ABOVE ADDRESS.

PORT DATE *(DD-MM-YYYY)*	**2. REPORT TYPE**	**3. DATES COVERED** *(From – To*
ır 04	**Master's Thesis**	1 Aug 02 – 26 Mar 04

TITLE AND SUBTITLE

ERFORMANCE STUDY OF TWO-STAGE-TO-ORBIT REUSABLE LAUNCH VEHICLE ULSION ALTERNATIVES

5a. CONTRACT NUMBER

5b. GRANT NUMBER

5c. PROGRAM ELEMENT NUMBER

AUTHOR(S)

, Marc, A., Captain, USAF

5d. PROJECT NUMBER
If funded, enter ENR #

5e. TASK NUMBER

5f. WORK UNIT NUMBER

RFORMING ORGANIZATION NAMES(S) AND ADDRESS(S)

r Force Institute of Technology
duate School of Engineering and Management (AFIT/EN)
0 Hobson Way
PAFB OH 45433-7765

8. PERFORMING ORGANIZATIO REPORT NUMBER

AFIT/GSS/ENY/04-M02

ONSORING/MONITORING AGENCY NAME(S) AND ADDRESS(ES)

RL/PRAT
tn: Dr. Dean Eklund
50 5th Street
dg 18D Room D232
PAFB OH 45433-7765 DSN: 785-0632

10. SPONSOR/MONITOR'S ACRONYM(S)

11. SPONSOR/MONITOR'S REP NUMBER(S)

STRIBUTION/AVAILABILITY STATEMENT

APPROVED FOR PUBLIC RELEASE; DISTRIBUTION UNLIMITED.

UPPLEMENTARY NOTES

BSTRACT

study investigated the performance of five Two-Stage-To-Orbit reusable launch vehicles (RLV), with stages propelled by rocket engines et engines and Rocket Based Combined Cycle (RBCC) engines. Horizontal versus vertical takeoff launch and direct versus lifting ascent ories were also studied. A method was conceived using a 3 degree of freedom optimization program, stage inert mass fractions, and a fi takeoff weight (GTOW) of 1,000,000 lbf to determine each RLVs performance based on payload weight delivered to orbit and total veh veight. RLV trajectory constraints, mass fractions, engine performance, and aerodynamics were assumed from literature of similar RLV rovided by the Air Force Research Laboratory (AFRL). The method devised accurately predicted performance for all RLVs studied, but ntensive and intolerant of small trajectory modifications. A horizontal takeoff RLV with the 1st stage powered by turbojet engines and ıge propelled by a rocket engine, in a lifting ascent trajectory, provided 3 times the payload weight to orbit when compared to the same e in a vertical takeoff mode. The RLV with both stages propelled by rocket engines lifted more payload weight into orbit with a lower t than all other RLVs studied. RLVs propelled by RBCC engines, on a direct ascent trajectory, had insufficient fuel to reach orbit becaus gh inert weight of the RBCC engines.

UBJECT TERMS

pace Propulsion, Rocket Propulsion, Jet Propulsion, Propulsion Systems

ECURITY CLASSIFICATION			**17. LIMITATION OF ABSTRACT**	**18. NUMBER OF PAGES**	**19a. NAME OF RESPONSIBLE PERSON**
T	**ABSTRACT**	**c. THIS PAGE**			Dr. Milton Franke
	U	**U**	**UU**	111	**19b. TELEPHONE NUMBER** *(Include area code)* (937) 255-6565, ext 4720; e-mail: milton.franke@afit.edu

Standard Form 298 (Rev: 8-98)
Prescribed by ANSI Std. Z39-18